Auditory Neuroscience, 1994, Vol 1, pp. 39–61
Reprints available directly from the publisher
Photocopying permitted by license only

Spectral Envelope Coding in Cat Primary Auditory Cortex: Properties of Ripple Transfer Functions

CHRISTOPH E. SCHREINER* and BARBARA M. CALHOUN

Coleman Laboratory, W. M. Keck Center for Integrative Neuroscience, University of California at San Francisco, San Francisco California 94143-0732

(Received August 8, 1994; accepted September 30, 1994)

Most of the functional aspects of the primary auditory cortex have been systematically explored using narrowband stimuli. Naturally occurring sounds are usually spectrally complex and not easily characterized by narrowband functions. In this study, the cortical response to a class of spectrally complex broadband stimuli is systematically explored. The stimulus is a harmonic series of components whose spectral envelope is sinusoidally modulated. We show that responses of neurons in the primary auditory cortex are influenced by a number of spectral envelope parameters, including the spacing of peaks in the spectral envelope, the phase of the envelope, and its modulation depth. Neuronal responses are also influenced by carrier properties, such as the specific spacings of the harmonic components, the total bandwidth of the stimulus, and the overall intensity. There is little apparent difference between the spectral envelope transfer functions, phase response profiles, and intensity response profiles for single and multiple units. The results suggest an additional approach for characterizing responses of neurons to broadband stimuli that are modeled after a behaviorally relevant class of sounds. Categorization of different types of responses to these stimuli is possible and can complement and expand the classic description of cortical receptive fields.

Key words: Primary auditory cortex, complex stimulus, spectral envelope, cat, transfer functions

THE STRUCTURE OF NATURALLY occurring sounds is frequently temporally and spectrally complex. Much of the exploration on the functional organization of the auditory cortex in mammals, however, has relied on the response to more simple stimuli, such as pure tones (Merzenich *et al.*, 1975; Reale and Imig, 1980; Phillips and Irvine, 1981; Phillips *et al.*, 1985; Schreiner and Mendelson, 1990; Schreiner *et al.*, 1992), and more parametrically accessible stimuli, such as amplitude modulated tones or noise (Phillips and Hall, 1987; Schreiner and Urbas, 1988; Phillips *et al.*, 1989; Eggermont, 1993), and frequency modulations (Suga and Jen, 1976; Mendelson and Cynader, 1985; Heil *et al.*, 1992b; Mendelson and Grasse, 1992; Mendelson *et al.* 1993). Using these stimuli, a number of organizational principles of auditory cortical fields, particularly of the primary auditory field (AI), have emerged that are likely to provide the basis for the processing of the more complex stimuli in the acoustic biotope of each animal. Among the findings were the discovery of a systematic frequency representation in AI (Woolsey and Watzl, 1942; Merzenich *et al.*, 1975), a nonuniform spatial distribution of the bandwidth of frequency tuning curves (Suga, 1965; Schreiner and Mendelson, 1990; Heil *et al.*, 1992b; Schreiner and Sutter, 1992), a nonuniform distribution of intensity-related responses (Suga, 1977; Asanuma *et al.*, 1983; Phillips *et al.*, 1985; Heil *et al.*, 1992b; Schreiner *et al.* 1992), a nonuniform distribution of inhibitory sideband characteristics (Shamma *et al.*, 1993; Sutter and Schreiner, 1990), preferential responses to specific frequency sweeps (Shamma *et al.*, 1992; Mendelson *et al.*, 1993), regions responsive to different binaural interaction cues (Imig and Adrian, 1977; Middlebrooks *et al.*, 1980), and regions sensitive to different spatial cues (Imig *et al.*, 1990, Rajan *et al.*, 1990a,b). Each of these studies directly describes receptive field properties for coding specific stimuli features, including spectral, temporal, and spatial characteristics. Similar observations have been made in the equivalent area, Field L, of birds (Langner *et al.*, 1981; Hose *et al.*, 1987; Heil *et al.*, 1992a).

However, the relationships between these basic functional organizations of cortical fields and the neuronal

Corresponding author: Dr. C. E. Schreiner, Coleman Lab, UCSF, Box 0732, San Francisco, CA 94143-0732.

responses to natural signals, as well as the coding principles of complex signals, such as environmental sounds and communication sounds, have not been well established. It is not yet evident whether the receptive field properties described for the coding of simple spectral, temporal, and sound localization cues are suitable and sufficient to predict the neuronal response to a large variety of complex signals. This is largely due to three limitations. First, the description of cortical coding properties has concentrated individually on spectral, temporal, and sound localization cues. For each of these cues, a number of descriptors have been used to characterize the corresponding receptive field aspects. However, it is not clear which of the currently used descriptors is necessary for a complete characterization of the receptive field and which of the parameters provide redundant or limited information. For example, the intensity dependence of a tonal response is usually characterized by the response threshold, the dynamic range, the best level, and an estimate of the monotonicity of the rate-level function. However, even a combination of all four descriptors is not sufficient to reconstruct fully the rate-level function and make predictions of the firing rate for arbitrary sound levels (Raggio and Schreiner, 1994).

Second, interactions between the three main aspects of auditory receptive fields, spectral, temporal, and spatial, have been insufficiently addressed. In other words, it is not clear whether the spectral, temporal, and spatial coding mechanisms operate independently and whether they can be characterized independently of each other.

Third, the high degree of temporal and spectral complexity of many natural or artificial signals renders the systematic definition and classification of relevant stimulus dimensions in those sounds difficult. Consequently, stimulus dimensions to describe receptive fields completely and appropriately in a systematic manner have not been fully identified.

This study begins to explore the cortical coding of a particular stimulus characteristic of broadband stimuli—the spectral envelope. It uses several characteristics of the spectral envelope that potentially carry much of the spectral information, including spacing between peak intensities, depth of modulation, overall intensity, and bandwidth. Many auditory stimuli, including most human vocalizations, music, and other naturally occurring and artificial sounds, are characterized by broadband spectra with distinctive, nonuniform spectral envelopes. Spectral envelopes are often essential for classification, as demonstrated by the distinct perceptual differences between various vowel sounds. Vowel spectra are characterized by several frequency regions with increased spectral energy (formants) separated by regions with decreased spectral energy. Different vowels are formed by altering the formant spacing or position (Dickson and Maue-Dickson, 1982). Figure 1 shows a spectral envelope for a human vowel sound and for a cat vocalization. Both vocalizations are marked by distinct maxima and minima in their spectral envelopes. Recent evidence from studies on the sharpness of tuning (Schreiner and Mendelson, 1990, Sutter and Schreiner, 1991; Schreiner and Sutter, 1992) and the distribution of inhibitory sidebands (Shamma *et al.*, 1993)

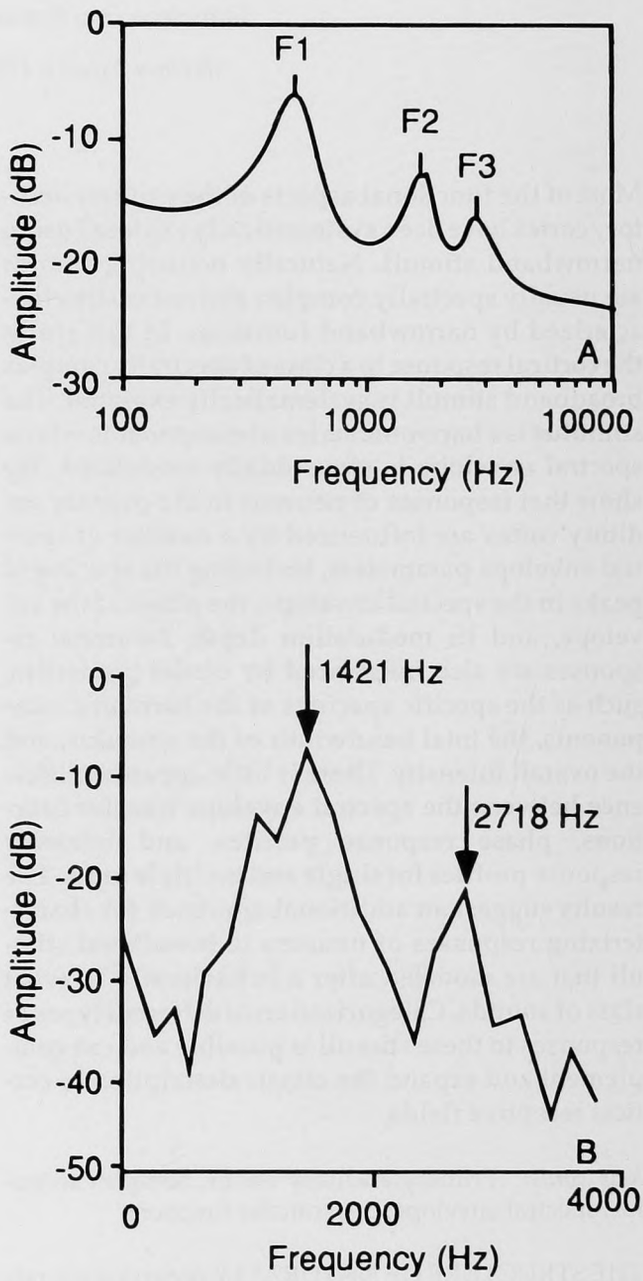

FIGURE 1 **Vocalizations.** (A) Schematized spectral envelope of a human vowel vocalization. The three formants are marked. (B) Actual spectral envelope of a cat vocalization. The two regions of highest energy are marked. Note that the two peaks are nearly 1 octave apart.

suggests that cortical neurons are able to distinguish between different spectral shapes.

One approach to generalize and parameterize this stimulus characteristic is the use of broadband spectra that have sinusoidal spectral envelopes with regard to logarithmic frequency and intensity scales. The benefits of ripple spectra as exploratory stimuli lie in: (1) an easy characterization of the spectral envelope that is parametrically accessible and resembles features of naturally occurring complex signals; (2) the fact that the stimulus characterization is largely independent of the spectral content and the location of the carrier signal; (3) its use as a tool for the exploration and characterization of the spectral receptive field using a broadband stimulus; (4) its potential use to compare these characterizations with those obtained with traditional methods, such as single and two-tone stimuli (Calhoun and Schreiner, 1993; Shamma *et al.*, 1994); and (5) its potential use as a stimulus to conduct a system-theoretical approach to the central auditory system that is equivalent to the spatial-frequency analysis used in the visual system and that may lead to an understanding of the processing of arbitrary spectral envelope wave forms (Hillier, 1991).

The spectral envelope of a ripple stimulus shares several important characteristics with luminance gratings commonly used to study processing in the visual system. Both stimuli provide similar distributed excitations across the receptor surface: in the visual system, the magnitude of the stimulus varies sinusoidally across the retina, whereas in the auditory system, the magnitude varies sinusoidally along the basilar membrane. Application of this method in the visual system has led to classifications of neurons by their response to sinusoidal gratings. Preferences to spatial characteristics of the stimulus, such as the grating frequency, modulation, and orientation, revealed important properties of central visual processing and provided a way of characterizing those properties.

In the first part of this study, we concentrate on characterizing the activity of cortical neurons and groups of neurons in the primary auditory cortex of the cat in response to ripple spectra for a range of ripple parameters, such as spectral envelope modulation frequency, phase, and modulation depth. The relationships of ripple spectrum responses to properties of spectral receptive fields as obtained with pure tones and the system-theoretically based derivation of spectral receptive fields from ripple transfer functions (RTFs) will be shown in forthcoming articles.

METHODS

Surgery and Animal Preparation

Data were collected from 22 healthy adult cats. Federal and institutional guidelines were followed in the care and use of the cats. The cats were pre-anesthetized using a mixture of ketamine hydrochloride (10 mg/kg) and acepromazine maleate (0.25 mg/kg). They were given dexamethasone sodium phosphate (0.25 mg/kg/24 h) to control brain edema and atropine sulfate (0.25 mg/12 h) to control mucous production. The femoral vein was exposed, and a venous cannulation was performed. After an initial dose of sodium pentobarbital (to effect, about 30 mg/kg), an areflexic, hydrated state was maintained through constant infusion of an 8:1 mixture of lactated Ringer's solution and sodium pentobarbital (about 4 mL/h) with supplemental intravenous injections of sodium pentobarbital as needed. A tracheal cannula was inserted. A rectal temperature probe was used to record the temperature of the animal and maintain it at 37.5°C using a feedback controlled heated water blanket. The electrocardiogram and respiration rate were remotely monitored throughout the experiment.

The head of the cat was fixed with a mouth bar, leaving the external meatuses unobstructed. The temporal muscle over the right hemisphere was then retracted. A craniotomy was used to expose the lateral cortex above the ectosylvian sulci. Finally, the primary auditory cortex was exposed by incising and reflecting the dura. The cortex was covered with silicon oil. For recording single units, the cortex was usually covered with a 1.5% solution of clear agarose in saline, which diminished cortical pulsations while providing a fairly unobstructed view of the cortical surface.

Hollow ear bars were inserted into the ear canals to deliver the stimuli and a micromanipulator was positioned so that an electrode could be inserted perpendicular to the surface of the cortex.

Electrophysiology

Parylene-coated tungsten electrodes (Microprobe) with an impedance of 0.8 to 1.2 MΩ at 1 kHz were inserted into the auditory cortex. A differential amplifier (DAM70-E, World Precision Instruments) filtered the activity below 1 kHz and above 10 kHz. A window discriminator (BAK DIS-1) permitted acceptable threshold levels and waveform criteria to be set to distinguish action potentials from the background signal. In this manner, responses of a single unit, or of multiple units, could be selected and recorded. Activity of an acceptable size and shape resulted in a trigger pulse that was sent to a computer (DEC 11/73) that recorded the number and time of the pulses to predetermined stimuli for later analysis.

Acoustic Stimuli

Experiments were conducted in a double-walled sound-shielded room (IAC). Auditory stimuli were generated with a stand-alone digital signal processor (DSP; TMS32010) with a 16-bit de-glitched DAC at a sampling

rate of 60 or 120 kHz. The stimulus was low-pass filtered 96 dB/octave at 15 or 50 kHz, respectively. The amplitude of tonal stimuli was controlled by the number of amplitude steps in the generating waveform. Each step corresponded to about 0.15 mV resulting in a dynamic range of 70 dB. To ensure a good signal-to-noise ratio for the complex sounds, the full amplitude was used for those conditions. Passive attenuators (Hewlett-Packard 350D) provided additional variable attenuation. The system was designed to provide a fairly flat transfer function when connected to the average cat ear (Sokolich, US Patent 4251686, 1981). Headphones (STAX 54) were enclosed in small chambers and connected to sound delivery tubes. The tubes were inserted into the acoustic meatuses. Two different types of stimuli were used: tonal stimuli and ripple stimuli. The tonal stimuli were used to determine the frequency response areas, whereas the ripple stimuli were used to determine the transfer functions and response profiles to spectrally complex signals.

Frequency Response Area

Using a manually controlled frequency generator (General Radio; 1309-A Oscillator) to search for a response, neurons between 600 and 1200 μm were identified. On finding a responsive single neuron or neuron cluster, the first step was to determine the frequency response area (FRA). After making an initial estimation of the characteristic frequency (CF) and bandwidth of the receptive field by manually varying the frequency and intensity and using audiovisual response criteria, the FRA was obtained by pseudorandomly presenting stimuli from 15 intensity levels and 45 frequencies. The levels were steps of 5 dB, giving a sampled dynamic range of 70 dB. The frequency range was centered around the manually determined CF of the recording site, and covered between 3 and 5 octaves, depending on the estimated bandwidth. The frequencies were spaced in equal fractions of an octave over the entire range. Each stimulus was presented for 50 ms with a 3 ms rise time and 400 ms interstimulus interval.

Ripple Spectra

Once the FRA was determined, the stimulus was changed from pure tones to broad band stimuli with distinct spectral envelopes. These stimuli will be referred to here as "ripple stimuli." The ripple stimulus is generated by sinusoidally modulating the spectral magnitude of a carrier along a logarithmic frequency scale. From 100 to 256 harmonic signals were used as carriers. The fundamental frequency of these harmonic components could be varied so that they usually ranged from 50 to 200 Hz and the maximum number of components was below 256 (the maximum number that could be produced by the DSP). The phase of the individual frequency components was fixed so that each component was phase shifted 53° farther than the previous one. This shifting eliminated strong peakiness in the temporal wave form that would have resulted with superposition of the components in cosine or sine phase. When plotting the spectrum on a double logarithmic scale, the spectral envelope of the stimulus was sinusoidal. Its bandwidth was set to 3 octaves with the geometric center of the band at a spectral maximum that usually was selected to correspond to the CF of the neuron. Since the individual components were linearly spaced, a 6 dB/octave decrease in the envelope of the ripple maintained a constant energy level per octave. The inverse wavelength of the sinusoidal spectral envelope is referred to as ripple density and is expressed in ripples/octave; the modulation of the spectral envelope is sinusoidal on a logarithmic scale and the standard spectral modulation depth (ripple depth) was 30 dB. The phase of the spectral envelope (ripple phase) is defined as 0° when the center peak of the spectral envelope at the geometric mean of the stimulus is aligned with the CF of the recording site. The overall intensity of the stimulus is expressed in dB sound pressure level (SPL) (as measured on the linear setting of a Bruel & Kjaer sound level meter at the end of the ear bars). The stimulus had a duration of 100 ms, including 5 ms rise and fall times. The interstimulus interval was usually 700 ms and was increased to 1 to 1.5 s if obvious adaptation effects were noted.

A schematic depiction of the standard stimulus, with a ripple density of 1 ripple/octave and a modulation depth of 30 dB, is shown in Figure 2A. Starting with the standard stimulus, individual parameters could be varied. For example, the ripple density can be changed (Fig. 2B) and the modulation depth can be varied (Fig. 2C). In addition, the overall intensity can be changed by increasing or decreasing each component by the same amount, and the fundamental frequency as well as the spectral width can be varied. As the ripple phase is varied, the central peak in the spectrum will move off the CF until a trough is aligned with the CF (Fig. 3), corresponding to a 180° phase shift. Note that envelope phase variations do not alter the frequency or phase properties of the carrier components, that is, the location of the carrier spectrum is not shifted. The amount of frequency shift (Δf, in octaves) of the apparent spectral peaks or troughs is determined by the ripple phase shift ($\Delta\Phi$) and the ripple density (RD):

$$\Delta f = (1/RD) * (-\Delta\Phi/360)$$

Ripple Transfer Function

RTFs express the firing rate in response to a ripple spectrum as a function of ripple density. To find an appropriate intensity for the stimulus, a ripple stimulus was presented with a modulation depth of 30 dB and a ripple density of 1 ripple/octave and the overall intensity was varied until the level evoking the strongest response

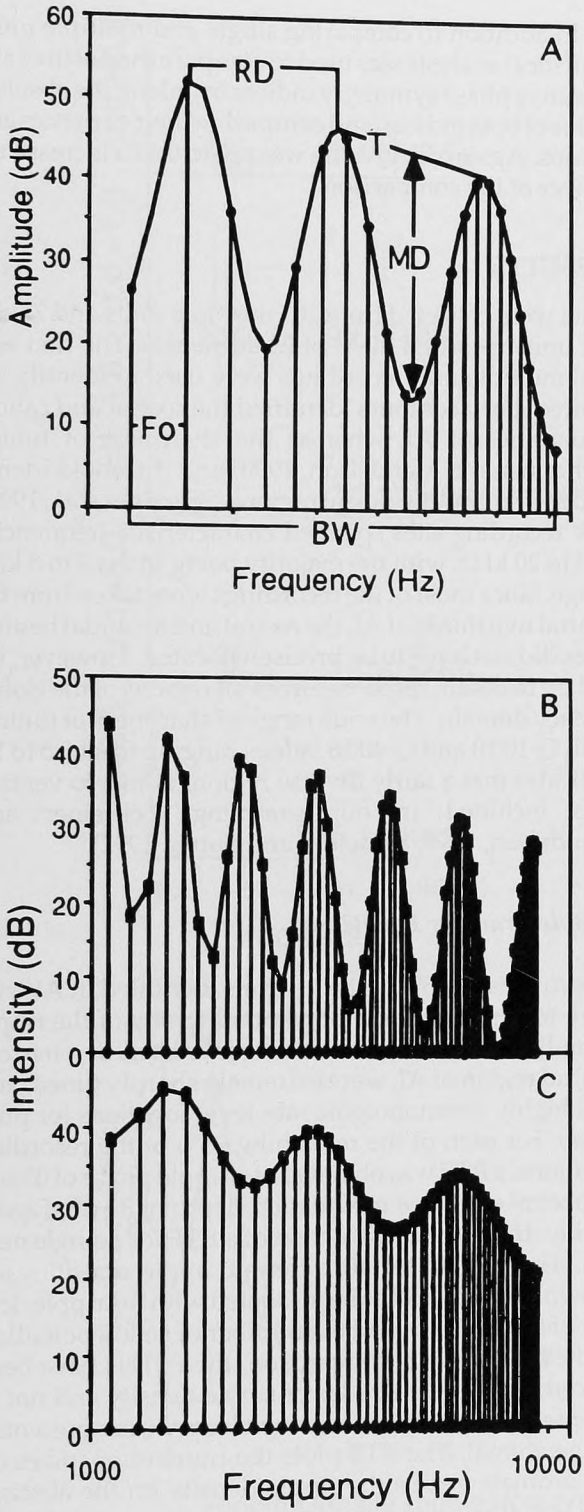

FIGURE 2 **Ripple stimulus.** (A) Standard stimulus: harmonic series of 100 to 200 components linearly spaced by the fundamental frequency (F_0) three octaves wide (BW), ripple density (spacing of peaks) of 1 ripple/octave (RD), modulation depth (amplitude of waveform) 30 dB (MD), and a 6 dB roll-off to maintain constant energy per octave (T). (B) Standard stimulus except ripple density has been changed to 2 ripples/octave. (C) Standard stimulus except modulation depth has been changed to 10 dB. Note that the amplitude maxima are the same, but the minima have changed.

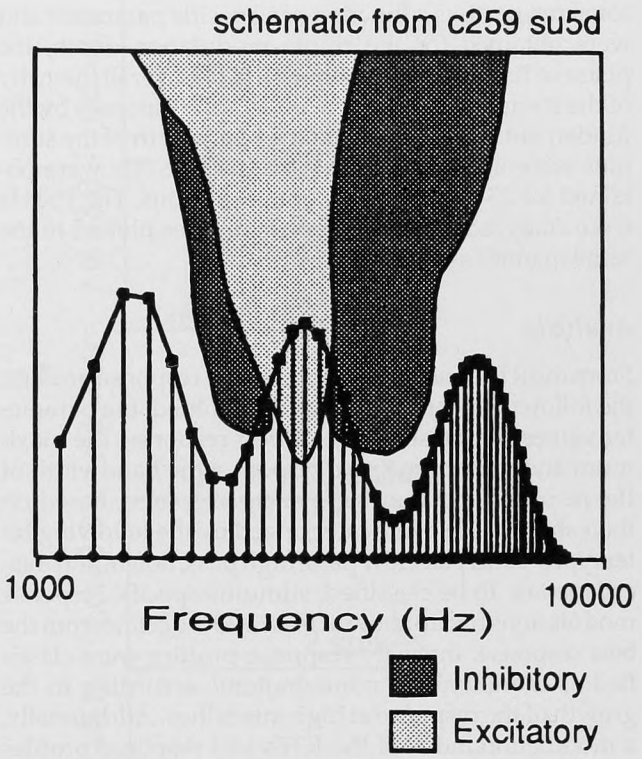

FIGURE 3 **Placement of ripple stimulus.** A schematic of a tuning curve shows the ripple stimulus positioned so that the center peak of the ripple stimulus is aligned with the characteristic frequency of the tuning curve. The tuning curve shows both the excitatory region (light gray), and the inhibitory regions (darker gray). With the center peak of the stimulus aligned with the characteristic frequency of the unit, the phase of the spectral envelope is considered 0°.

was determined using an audiovisual measure of response. This best intensity was used to obtain the RTFs.

Data were collected for an ordered sequence of ripple densities (15 values; 0 to 6 ripples/octave 0.2 to 1 ripples/octave spacing) or a pseudorandom sequence (14 or 20 values; 0 to 8.66 ripples/octave; 0.33 to 0.66 ripples/octave spacing). Each stimulus condition was presented 25 times. To minimize adaptation to a particular stimulus, the interstimulus interval was at least 700 ms, and occasionally more than 1. In most cases, this long interstimulus interval allowed the responses to the stimuli to be equally strong at the end of the 25 presentations as at the beginning.

The data were collected in poststimulus time histograms (PSTHs) allowing the number of action potentials and latency of each response to be determined. To create the ripple transfer functions from the PSTHs, the number of responses in each PSTH are determined. Since tonic responses were not seen, we only consider the number of spikes in a 30 ms window that begins with the first spike after the onset of the stimulus.

Once the standard RTF was determined, response profiles were created for several other stimulus parameters. Response profiles plot the strength of the neu-

ronal response as a function of a specific parameter and were obtained for the ripple modulation depth, the phase of the spectral envelope, and the overall intensity of the stimulus. In addition, effects on responses by the fundamental frequency and the bandwidth of the stimulus were investigated. In each case, PSTHs were obtained for 25 presentations of the stimulus. The PSTHs were analyzed and the response profiles plotted in the same manner as for the RTFs.

Analysis

From the RTFs and, if appropriate, the response profiles, the following properties were determined: the parameter values for the strongest or best response, the maximum and minimum spike response, the bandwidth of the response and the shape of the response. Based on their shape, RTFs were categorized by the following filter types: band pass, low pass, high pass, notch, and miscellaneous. To be classified, stimulus-specific response modulations had to show at least a 30% decline from the best response. Intensity response profiles were classified as monotonic or nonmonotonic according to the growth of the response at high intensities. Additionally, a modulation index of the RTFs and response profiles was determined by dividing the difference between the maximum and minimum response by the maximum response. This index varies between 0 and 1 and reflects the degree of response modulation due to changes in the varied parameter. The modulation index was determined for RTFs (ripple modulation index [RMI]) and for the phase profiles (phase modulation index [PMI]). The best response of a RTF or a response profile was the value of the variable parameter that elicited the strongest response. If two neighboring parameter values elicited identical responses, their values were averaged. The maximum response was the largest number of spikes that occurred following a stimulus onset. The minimum response was the average of the three parameter values that elicited the lowest number of spikes following stimulus onset. The bandwidth of an RTF is defined as the range of ripple densities over which the response is larger than the 50% value between maximum and minimum response.

When possible, analyses were carried out individually for single unit and multiple unit recording sites and compared to each other. First, the variance and the mean of the two populations were determined. Then a variance ratio test was used to determine whether the variances of the two populations were the same, and a *t* test was used to compare the means of the two populations. To increase the power of the test, and reduce the possibility of false-negative results, $\alpha = 0.1$ was used for the test value. To compare the frequency distribution of filter classifications, a contingency table was set up and the chi-square test was used.

In addition to comparing single and multiple units, statistical analysis was used to compare the positive and negative phase symmetry indices by taking the absolute value of both indices, and comparing their variances and means. Again, the α value was set to 0.1 to increase the power of the comparison.

RESULTS

Data were collected from 201 multiple units and 77 single units recorded in AI of 22 adult cats. The first several multiple unit recordings were used to identify AI. Isofrequency contours identified the rostral and caudal boundaries of AI, whereas the sharpness of tuning (Schreiner and Mendelson, 1990) and threshold identified the ventral and dorsal regions (Schreiner *et al.*, 1992). The recording sites spanned characteristic frequencies of 1 to 20 kHz, with the majority being in the 3 to 8 kHz range. Since most of the recordings were taken from the central two thirds of AI, the rostral and arcaudal boundaries did not have to be precisely located. However, we did try to obtain responses from all regions of the isofrequency domain. The wide range of sharpness of tuning, with Q-10dB and Q-40dB values ranging from 0.5 to 10, indicates that a fairly diverse region, dorsal to ventral, was included in our sampling (Schreiner and Mendelson, 1990; Schreiner and Sutter, 1992).

Ripple Transfer Functions

Approximately 5% of the neurons identified in AI with pure-tone stimuli did not respond to any of the ripple stimuli. All of these neurons were located in a narrow central region of AI, were extremely sharply tuned, and had highly nonmonotonic rate-level functions for pure tones. For each of the remaining 95% of the recording locations, a RTF was obtained at a ripple phase of 0° and a spectral envelope modulation depth of 30 dB. Figure 4A illustrates the construction of a RTF for a single neuron. The PSTHs for 10 different ripple densities are shown. Each PSTH has been labeled with the ripple density of the stimulus and the number of action potentials elicited. For ease in comparison, the PSTHs have been placed in ascending order of ripple density and not in the pseudorandom order in which they were presented to the animal. The RTF plots the number of spikes on the ordinate versus the ripple density on the abscissa (Fig. 4B). The filled points represent one set of 10 stimuli; the open points represent a second, complementary set of 10 stimuli. The line represents a two-point average of the full data set. Several common properties of RTFs can be illustrated with this example, including a best ripple density, the filter shape, the bandwidth of the response, and the modulation index. Commonly, the RTF reveals a range of ripple densities for which the re-

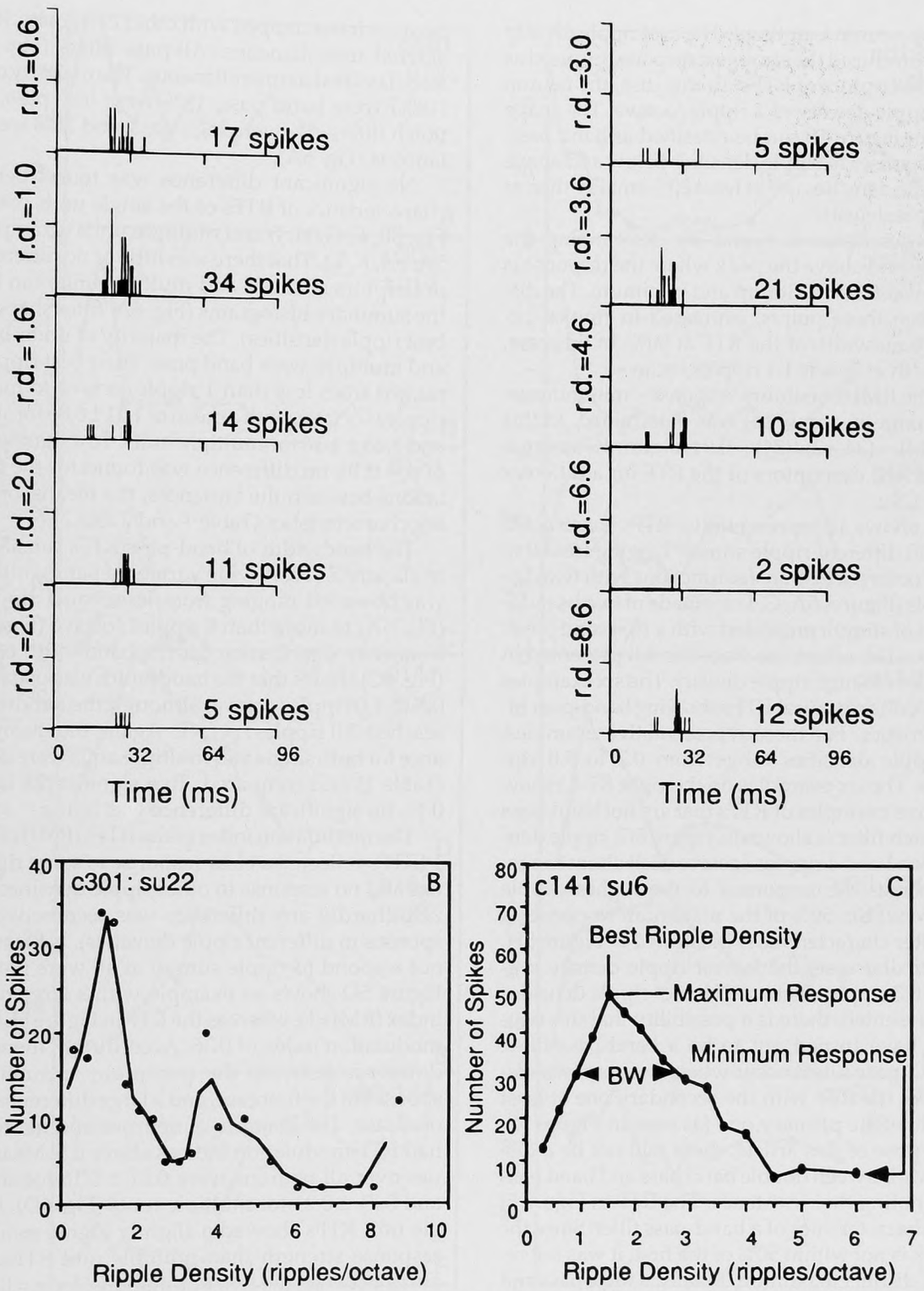

FIGURE 4 **Ripple transfer functions.** (A) Poststimulus time histograms showing the responses of a unit at different ripple densities. The number of responses and the ripple density are shown next to each plot. Although the stimuli were presented in a pseudorandom order, they have been ordered here for ease in interpretation. (B) The ripple transfer function plots the number of spikes at each ripple density against the ripple density. The open circles illustrate one set of 10 pseudorandom stimuli, the closed circles represent a second set. The line is a two-point average of the points. (C) A ripple transfer function shows that the best ripple density is 1.5 ripples/octave, the maximum response is 50 spikes, and the minimum response is 7 spikes. The bandwidth (BW) is the ripple densities over which the response is greater than half way between the maximum and minimum response: in this case, 1.0 to 2.8, or 1.8 ripples/octave. The modulation index is the difference between the maximum and the minimum, divided by the maximum: (50 – 7)/50 = 0.86.

sponse of the neuron is optimal. The best ripple density (that which produced the strongest response), is used as one of the descriptors of RTFs. In this case, the neuron has a best ripple density of 1 ripple/octave. The shape of the RTF in Figure 4B can be classified as band pass, since the responses to ripple densities below and above the best ripple densities are at least 30% smaller than at the best ripple density.

Another descriptor is found by determining the points below and above the peak where the response is halfway between its maximum and minimum. The distance between these points, expressed in ripples/octave, is the bandwidth of the RTF at 50%. In this case, the bandwidth at 50% is 1.1 ripples/octave.

Finally, the RMI (maximum response – minimum response)/maximum response) was determined. In this example, RMI = (34 – 2)/(34) = 0.94. Figure 4C summarizes the various descriptors of the RTF for a different neuron.

Figure 5 shows 12 representative RTFs constructed from 14 to 20 different ripple stimuli ranging from 0 to 8.6 ripples/octave. The transfer functions with two distinct symbols (Figures 5A, G, I) are made of two pseudorandom sets of stimuli presented with a 15 second break between sets. The others are from stimuli presented in order from low to high ripple density. The six examples on the left (A–F) are typical RTFs showing band-pass filter characteristics. For these representative examples, the best ripple densities range from 0.7 to 5.0 ripples/octave. The six examples on the right (G–L) show representative examples of RTFs that are not band-pass filters. A notch filter is shown in Figure 5G: ripple densities between 1 and 4 ripples/octave elicit almost no response, whereas the responses to the highest ripple densities are within 50% of the maximum response. A low-pass filter characteristic is illustrated in Figure 5H. In this particular case, the lowest ripple density presented was 0.3 ripples/octave. If lower ripple densities had been presented, there is a possibility that this neuron would have turned out to be a band-pass filter. Double band-pass filters occur when there are two distinct peaks in the RTF with the secondary one at least 50% as high as the primary one (as seen in Figure 5I). For the purpose of this article, there will not be a distinction made between double band pass and band pass aside from noting their existence. The RTF in Figure 5J shows the characteristics of a band-pass filter. Since the second peak is not within 50% of the first, it was not regarded as a distinct maximum. Finally, a high-pass and an all-pass filter are shown in Figure 5K and 5L, respectively. Obviously, in determining the type of filter, there is always some overlap, and approximation. For instance, unless a ripple density of 0 ripples/octave was presented, a low-pass filter could actually be misclassified as a band-pass filter. If a filter did not have a clear classification, either because the data were too noisy or because it overlapped with other categories, it was considered miscellaneous. All-pass filters (Fig. 5L) were also classified as miscellaneous. The majority of neurons (48%) were band pass, 18% were low pass, 6% were notch filters, 3% were high pass, and 25% were miscellaneous (Fig. 6A).

No significant difference was found between the characteristics of RTFs of the single units (examples in Fig. 5B, E, G, H, J) and multiple units (examples in Fig. 5A, F, I, K, L). That there was little or no difference in the descriptors of single and multiple units can be seen in the summary histograms (Fig. 6A: filter shapes; Fig. 6B: best ripple densities). The majority of units, both single and multiple, were band pass. Their best ripple density ranged from less than 1 ripple/octave to more than 4 ripples/octave, with a mean of 1.11 ± 0.86 for single units and 1.25 ± 1.16 for multiple units. To a significance level of $p = 0.10$, no difference was found for the two populations between the variances, the means, or the filtering characteristics (Table 1 and Table 2).

The bandwidth of band-pass RTFs can also be used to classify RTFs. A wide variety of bandwidths of RTFs was observed ranging from less than 1 ripple/octave (Fig. 5A) to more than 3 ripples/octave (Figs. 5E, F). A frequency distribution for the bandwidth of the RTFs (Fig. 6C) shows that the bandwidth was usually around 0.5 to 1.0 ripple/octave, although the bandwidth often reached 3.0 ripples/octave. Again, the mean and variance for both single and multiple units were determined (Table 1) and compared. To a significance level of $p = 0.10$, no significant difference was found.

The modulation index of the RTFs (RMI) ranged from 1 (RTFs reflected a clear response to some ripple densities and no response to other ripple densities) to nearly zero (hardly any difference was seen between the responses to different ripple densities). Neurons that did not respond to ripple stimuli at all were not included. Figure 5C shows an example with a large modulation index (RMI=1), whereas the RTF in Figure 5L has a small modulation index of 0.36. Accordingly, there is a small difference between the maximum and minimum responses in the first case, and a large difference in the second case. The majority of neurons and neuron clusters had RTF modulation indices above 0.5. Mean RMI values over all neurons were 0.81 ± 0.16 for single units, and 0.71 ± 0.21 for multiple units (Fig. 6D), that is, single unit RTFs showed a slightly higher modulation of response strength than multiple unit RTFs. The variances between the two populations, for $p = 0.1$, showed a significant difference, indicating that the populations were different. However, there was no significant difference between the means (Table 1).

In summary, the systematic investigation of the influence of a range of spectral envelope frequencies on cortical responses to broadband stimuli revealed that (1) the majority of cortical neurons are tuned to a specific

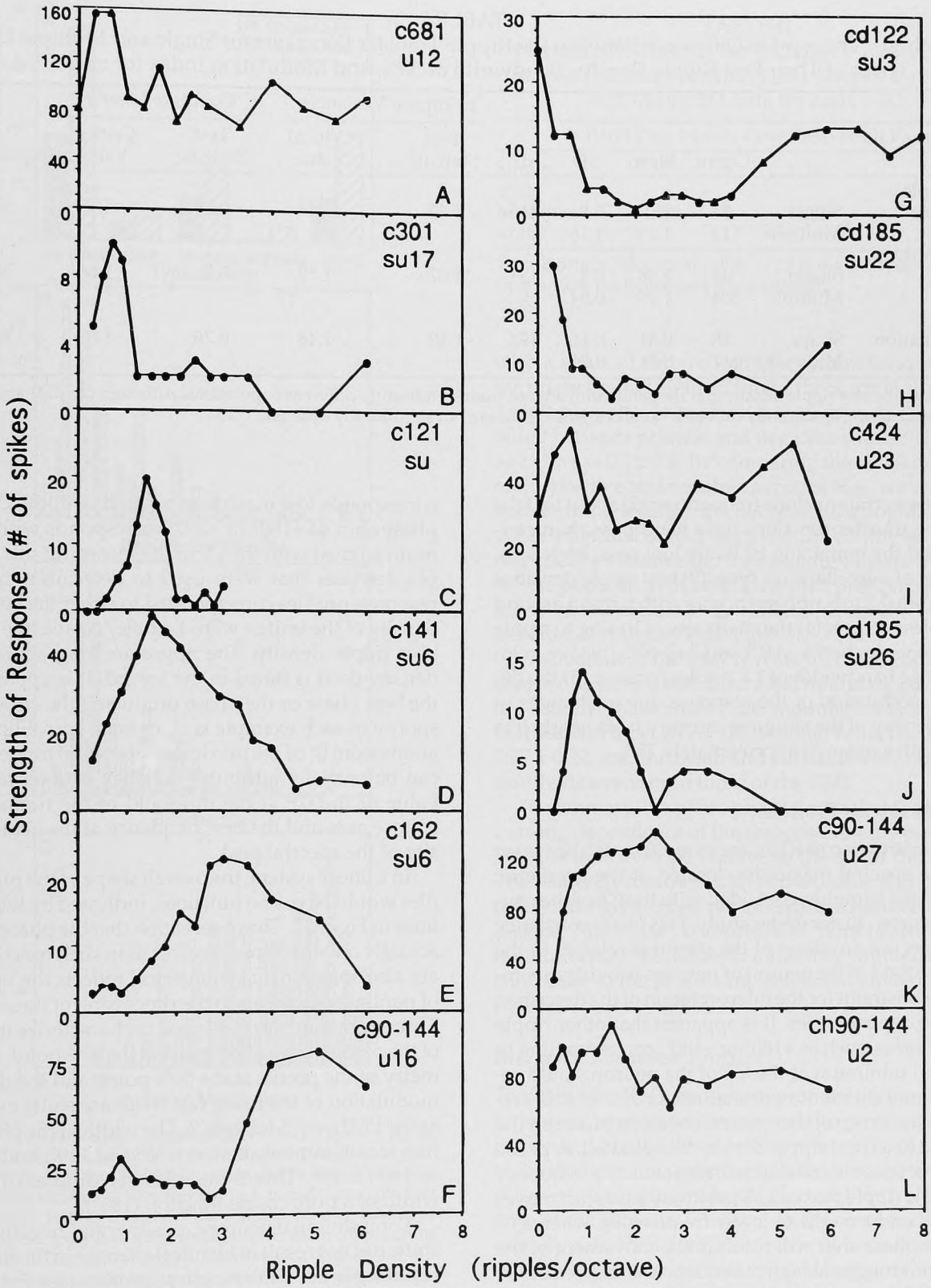

FIGURE 5 **Ripple transfer functions.** Twelve different ripple transfer functions showing typical shapes. The plots were determined by using ripple stimuli with modulation depths of 30 dB. The fundamental frequency was constant for each plot. (A-F) Typical band-pass filters with the best ripple density ranging from 0.5 to 5.0 ripples/octave. (G) Notch filter, (H) Low-pass filter (I) Double-band pass. These are counted as band pass, and the best ripple density is the overall best response. (I) Band-pass filter. (K) High-pass filter. The response at the highest ripple densities never fell below 50% of the maximum response. (L) A mixed response, or all-pass.

TABLE I
Hypothesis: There is No Difference Between the Ripple Transfer Functions for Single and Multiple Units in Terms of Their Best Ripple Density, Bandwidth at 50%, and Modulation Index for an $\alpha = 0.1$

						Compare Variances		Compare Means		
		Count	Mean	SD	df	Test Statistic	Critical Value	Test Statistic	Critical Value	Significance
Best ripple density	Single	54	1. 11	0.86	165	1.47	1.48	0.54	1.65	No
	Multiple	113	1.25	1.16						
Bandwidth at 50%	Single	49	1.36	0.8	151	1.07	1.52	0.26	1.66	No
	Multiple	104	1.29	0.84						
Ripple modulation index	Single	58	0.81	0.16	173	1.49	1.48	0.76	1.65	Yes
	Multiple	117	0.71	0.21						

Conclusion: the best ripple density and the bandwidth are not from significantly different populations. Although the RMI are from different populations (significantly different variances), the means are not significantly different.

range of spectral envelope frequencies; (2) about half the envelope transfer functions have band-pass characteristics, and the remaining RTFs are low pass, high pass, notch, or of miscellaneous type; (3) best ripple densities range from 0.3 to 5 ripples/octave with a mean around 1.2 ripples/octave; (4) the sharpness of tuning to ripple densities varies between 0.3 and 3 ripples/octave, with an average bandwidth of 1.3 ripples/octave; (5) the degree of modulation of the response due to changes in ripple density of the stimulus can vary from nearly 0 to 100%, with a mean of approximately 75%.

Phase Response Profiles

In the construction of RTFs, the stimulus was always set so that a spectral maximum, located at the geometric center of the stimulus, coincided with the CF of the neuron or neuron cluster under study. This phase constancy of the spectral envelope of the stimulus relative to the receptive field of the neuron or neurons provides an important constraint for the interpretation of the described response dependencies. It is apparent that other ripple phase choices, such as +180° or −180°, corresponding to a spectral minimum at the CF of the neuron, could result in quite different neuronal responses. In this section, the influence of the spectral envelope phase on the response to a fixed ripple density is evaluated. A phase shift of the spectral envelope corresponds to a frequency shift of the ripple maxima. A positive phase shift moves all peaks and troughs to lower frequencies, whereas a negative phase shift will result in the movement of the peaks and troughs to higher frequencies. The frequency content of the carrier spectrum does not change with these phase shifts.

Figure 7 shows the phase response profile, the spike count versus the ripple phase of the stimulus, for six different recording sites. In each case, a phase shift of 0° corresponds to a maximum aligned with the CF, and a phase shift of +180° or −180° corresponds with a minimum aligned with the CF of the recording site. The ripple densities that were used to determine the phase response profiles corresponded to either the best ripple density of the unit or were 1 ripple/octave, the average best ripple density. The approximating actual ripple density used is stated in the legend. It is apparent that the best phase or the phase producing the strongest response in each example is at, or near, zero. Slight deviations from 0° of the maximum of several phase profiles can be partially attributed to small differences in the value of the CF at the threshold of the frequency response area and the best frequency at the actual intensity of the spectral peak.

In a linear system, the overall shape of the phase profiles would be cosine functions, indicated by the dashed lines in Figure 7. The observation that the phase profiles actually obtained are narrower than such functions and are also somewhat asymmetrical reflects the operation of nonlinear elements in the processing of these stimuli. Three parameters will be used to characterize the shape of the phase profiles: the width at the 50% point, the symmetry of the profile at the 50% point, and the degree of modulation of the firing rate by phase shifts expressed as the PMI (see "Methods"). The width of the phase profiles was commonly between 60° and 140°, with a mean of 100° ± 29°. This is significantly different from the width of a pure cosine function (180°).

For individual neurons, positive and negative phase shifts did not result in identical changes in the firing rate resulting in asymmetric phase profiles (see Fig. 8). This behavior is quantified by the symmetry index (SI). This index was found by determining the positive and negative phase shifts required to reduce the response by 50% and then calculating SI as follows: $SI = (\Phi_{pos} - \Phi_{neg})/(\Phi_{pos} + \Phi_{neg})$. Values of SI can vary from +1 to −1,

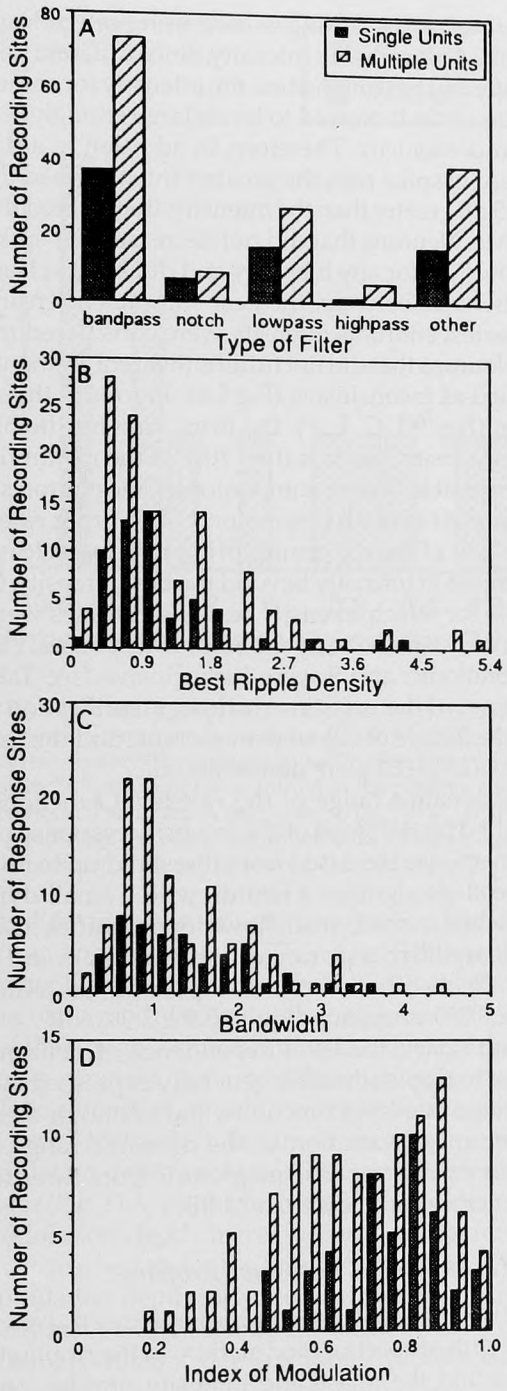

FIGURE 6 **Frequency distributions**. (A) Filter types. Histograms show the number of units that are classified in each particular filter type for single units and multiple units. There was no significant difference between the two populations. (B) Best ripple density. Histograms show the number of units that have each of the best ripple densities for single units and multiple units. The bin size is 0.3 ripples/octave. There was no significant difference between the mean and variance for these two populations. (C) Bandwidth of ripple transfer functions (RTFs). Histograms showing the number of units having the specified RTF bandwidths for single units and multiple units. The bin size is 0.25 ripples/octave. (D) Index of modulation. Histograms showing the number of units having the specified index of modulation for single units and multiple units. The bin size is 0.05.

TABLE II
Hypothesis: There Is No Difference Between the Ripple Transfer Function Filter Shapes for Single and Multiple Units for an $\alpha = 0.1$

	Band Pass	Notch	Low Pass	High Pass	Mixed
Single units	37	6	16	1	16
Multiple units	75	8	27	5	41

Test statistic = 2.3; critical value = 13.3 (for $\alpha > 0.1$, df = 8).
Conclusion: the hypothesis is not rejected.

with a value of zero reflecting a symmetrical shape of the phase profile. Figure 8 shows the SI for 11 single and 1 multiple units. The responses were nearly equally divided between positive and negative values. The average SI was -0.1 ± 0.4. By comparing the absolute values of the positive and negative asymmetries, we were able to determine whether the neurons, as a population, favored one direction or behaved differently in one direction. The variance and the absolute value of the mean for the population of neurons with a positive asymmetry were not significantly different from those with a negative asymmetry (see Table 3).

Evaluation of the PMI reveals that most phase profiles in our sample exhibited a full modulation of the firing rate by phase shifts. This modulation is similar to that seen for most RTFs. The average value for PMI was 0.77 ± 0.22, and the mean and variance were not significantly different from those of the RMI.

In summary, the phase profiles revealed that there is a strong dependence of the responses on the position of the spectral envelope relative to the CF of the neuron. The relatively narrow width of the profile and its asymmetry strongly suggest the influence of nonlinear mechanisms, such as compressive nonlinearities and nonuniformly distributed inhibitory influences that contribute to the processing of spectral envelope information.

Intensity Response Profiles

To determine RTFs and phase profiles, audiovisual criteria were used to set the intensity to produce a strong response. Usually, this intensity was approximately 15 to 25 dB above the response threshold for the tested ripple density (ripple phase, 0°). To test the overall influence of the stimulus intensity on the response to ripple stimuli, rate-level functions were obtained for ripple densities at or near the best ripple density of the neuron or neuron group. Figure 9 shows six examples of rate-level functions. Neurons were classified as monotonic, nonmonotonic, or inconclusive. For nonmonotonic neurons, the firing rate peaked for a specific best intensity, and then proceeded to decrease. Nonmonotonic neurons

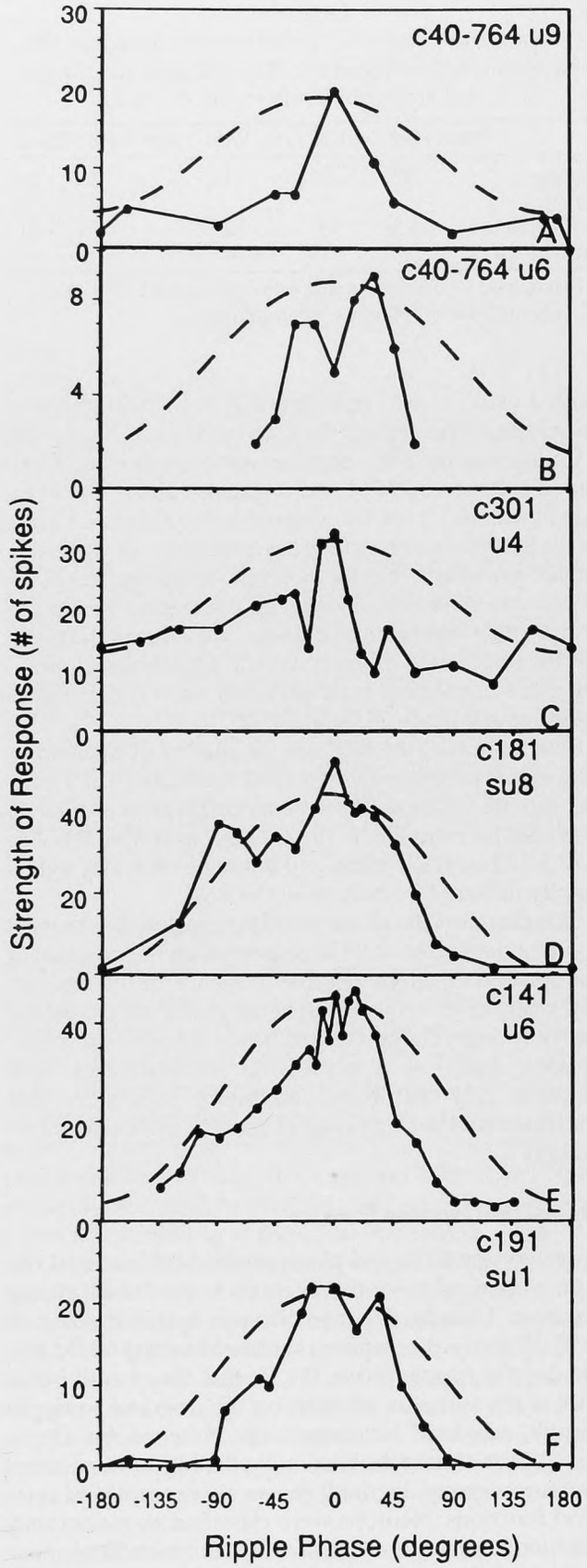

are defined as decreasing in their firing rate at least 30% with a 15 dB increase in intensity. Since different neurons had different best intensities, the intensity for some stimuli were never increased to levels large enough to determine monotonicity. Therefore, in addition to a definite decrease in spike rate, the greatest intensity had to be at least 15 dB greater than the intensity that elicited the best response. Neurons that did not decrease their spike rate to below 70% for any intensity and did have at least a 15 dB difference between the best stimulus intensity and the greatest stimulus intensity were considered monotonic. Neurons that did not fulfill either requirement were classified as inconclusive (Fig 9A). In four of the six examples (Fig. 9B, C, E, F), the firing rate for the highest tested intensity was less than 70% of the maximum firing rate; that is, were nonmonotonic. The neuron shown in Figure 9D is clearly monotonic. The firing rate stays above 70% of the maximum firing rate for at least a 30 dB increase in intensity beyond the best intensity. Of the 42 units for which intensity response profiles were collected, only 8 had clearly monotonic responses, 25 were nonmonotonic, and 9 were inconclusive (see Table 4). Therefore, of the units in which an identification could be made, 24% (8 of 33) were monotonic and the remaining 76% (25 of 33) were nonmonotonic.

The dynamic range of the rate-level functions was quantified by the slope of the intensity response profile as the response increased from threshold up to its peak. A large slope signifies a neuron with a small dynamic range while a small, or shallow slope signifies a neuron with a large dynamic range. The histogram in Fig. 10 shows the distribution of the slopes and has a mean of 0.058 ± 0.029 corresponding to $5.8 \pm 2.9\%$/dB.

In summary, the level dependence of neuronal responses to ripple stimuli is generally expressed by nonmonotonic rate-level functions, and although there is a fair amount of variation in the dynamic range, most units vary their response magnitude from threshold to a peak response in less than 20 dB.

Modulation Depth Response Profiles

One of the principal descriptors of the spectral envelope is the depth of spectral modulation. In the ripple stimuli used to find the phase and intensity profiles, and the RTFs, the modulation depth was uniformly set to 30 dB. To determine the modulation depth response profiles, the ripple density, intensity, and phase were set, and the modulation depth was varied. The ripple density was set at, or near, the best ripple density, the phase was set

FIGURE 7 **Phase shifts.** Responses of six single units as the phase of the spectral envelope is varied. A phase shift of zero corresponds to the center peak of the stimulus being aligned with the CF of unit. The dotted line is a sinusoid fit between the maximum and the minimum response. The modulation depth for all the stimuli was 30 dB. The ripple densities (rd) were as follows: (A) rd = 1.0; (B) rd = 1.0; (C) rd = 1.0; (D) rd = 1.8; (E) rd = 1.8; (F) rd = 1.7.

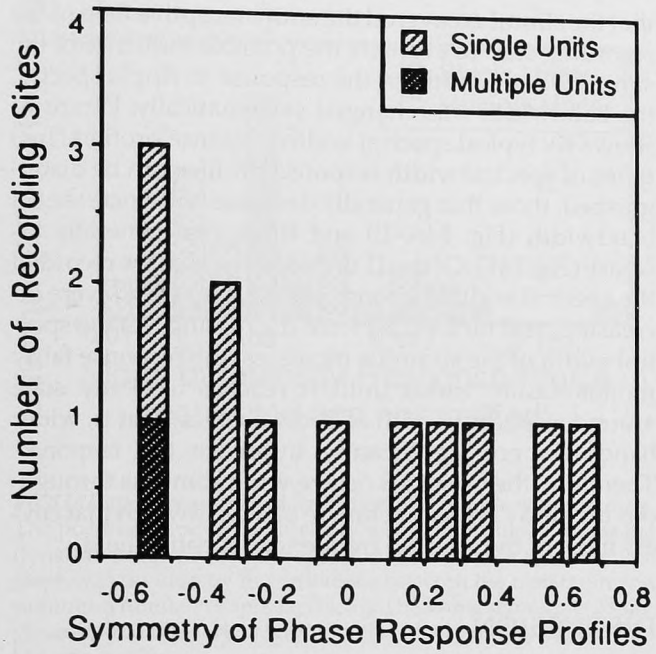

FIGURE 8 **Frequency distribution for phase symmetry index.** To determine the symmetry of a phase response profile, the symmetry index considers the phase required to reduce the maximum response by 50% as the phase is shifted in the positive and negative directions. The index is $(\phi_{pos} - \phi_{neg})/(\phi_{pos} + \phi_{neg})$. The light hatching indicates the phase asymmetry for 11 single units and the dark hatching, for 1 multiple unit. The bin size is 0.1.

to 0°, and the intensity was the same as for determining the RTF and phase response. Then 6 to 10 different modulation depths were presented between 0 and 40 dB. An increase of the modulation depth corresponded to a lowering of the troughs while keeping the levels of the spectral peaks constant. As a consequence, an increase in modulation depth resulted in a slight decrease in total energy (see "Methods"). Figure 11 shows six examples of modulation depth profiles. As shown in the first five examples (Fig. 11A–E), the response usually increases as the modulation depth increases until a maximum or plateau is reached at depths ranging from 5 to 30 dB. As the modulation depth increased further, the firing rate was fairly independent of modulation depths. Figure 11F shows two modulation depth response profiles taken for the same unit. The closed circles were taken using the best ripple density of 1.0 ripple/octave and the open circles used a ripple density of 3.0 ripples/octave. The clear differences between the two profiles indicate that the depth profile depends on the ripple density used. Figure 12 shows the frequency distribution for the lowest of the near optimal (best) modulation depths, at the best ripple density of the unit. The mean best modulation depth was 20 ± 8dB. For most units, however, a modulation depth of 30 dB still produced near optimal responses. Therefore, this modulation depth was selected for obtaining most RTFs and other response profiles.

Fundamental Frequency Response Profile

The ripple stimulus used in this study consisted of a series of harmonically related components. The fundamental frequency of the harmonic complex was chosen so that the complex contained at least 126 components and maximally 256 components. As a consequence, the lowest octave of the 3-octave wide stimulus contained at least 18 and maximally 36 components, thereby providing an adequate representation of the sinusoidal spectral envelope (see Fig. 1). The fundamental frequencies actually used for obtaining RTFs and response profiles ranged from 37.5 to 150Hz. To estimate systematically the influence of variations of the fundamental frequency on the response to a ripple stimulus, we varied the fundamental frequency over a wide range for 12 neurons. The fundamental frequency response profiles in Figure 13 illustrate that there were definite changes in the responsiveness as the fundamental frequency varied. For higher fundamental frequencies, the spectral envelope slope is undersampled, especially for high ripple densities, and is no longer well represented. Therefore, it is reasonable to expect that, at high fundamental frequencies, there are fairly large variations in the response magnitude. The reason for the variations at low fundamental frequencies (see Fig 13A, C, F) is less clear and suggests a reliance of the response on the fundamental frequency itself, rather than exclusively on aspects of the spectral envelope. Fundamentals ranging from 100 to 1000 Hz (at which frequency the spectral envelope is being grossly undersampled) elicited strongest responses. No common pattern for fundamental frequency response profiles was apparent.

Spectral Width Response Profiles

Finally, the influence of the spectral width of the ripple stimulus was investigated. In all previous conditions, it was set to 3 octaves. This width was chosen to ensure

TABLE III

Hypothesis: There Is No Difference Between the Positive and Negative Asymmetries for an $\alpha = 0.1$

					Compare Variances		Compare Means	
Asymmetry	Count	Mean	SD	df	Test Statistic	Critical Value	Test Statistic	Critical Value
Positive	5	0.352	0.2	10	0.276	1.8	1.29	3.97
Negative	7	0.429	0.19					

Test statistic = 0.28; critical value = 1.8 (for $\alpha > 0.1$, df = 10). Conclusion: the hypothesis is not rejected.

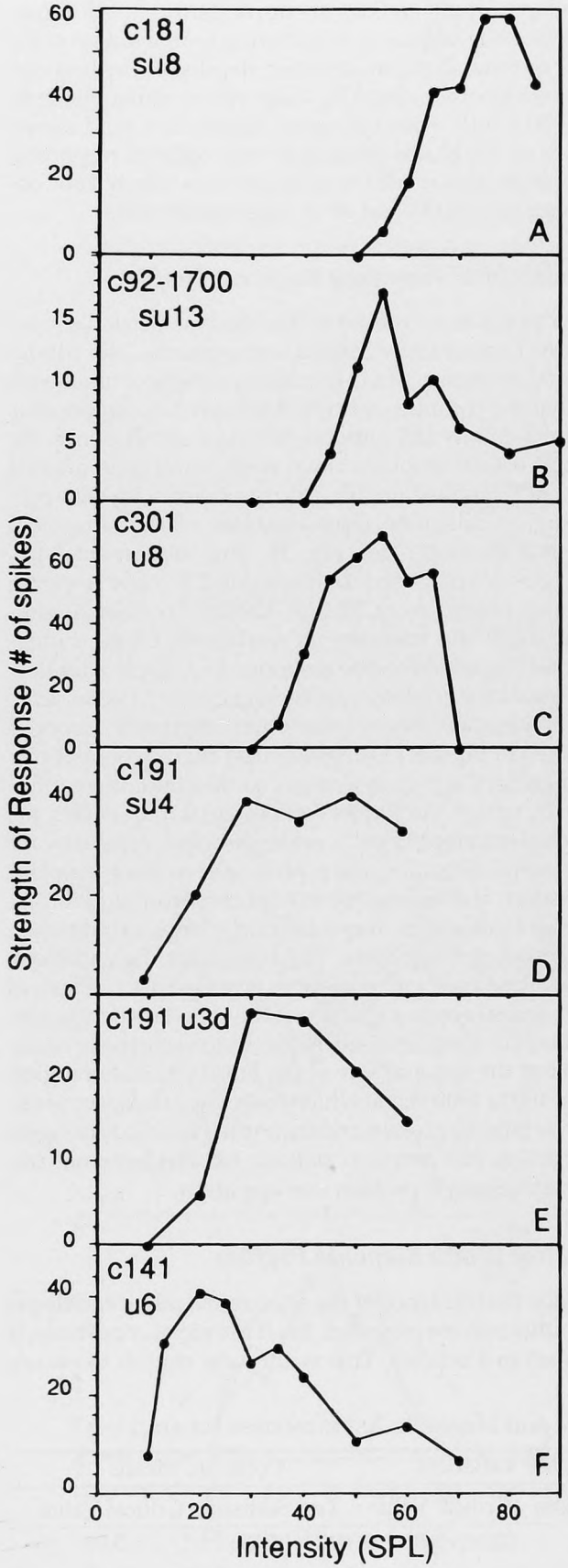

that the stimulus covered the entire receptive field of the recording site. To evaluate the possible influence of the stimulus bandwidth on the response to ripple spectra, the bandwidth was changed systematically. Figure 14 shows six typical spectral width response profiles. Two types of spectral width response profiles can be distinguished: those that generally decrease with increases in bandwidth (Fig. 14A–E) and those that generally increase (Fig. 14F). Of the 11 units from which we recorded the spectral width response profile, two (18%) were increasing, and nine (82%) were decreasing. As the spectral width of the stimulus increases, the response fairly monotonically varies until it reaches a steady state around a spectral width of 2 to 3 octaves, that is, wider bands do not significantly influence the response. Therefore, the use of a 3 octave wide stimulus throughout the study is a safe estimate of a bandwidth that covers most of the affected frequency receptive field.

DISCUSSION

This series of experiments was conducted to investigate the response of primary auditory cortical neurons to broadband sounds with distinct spectral envelopes. In particular, it was designed to determine whether neurons in AI are sensitive to specific attributes of sinusoidal spectral envelopes, and which are the most salient features of spectral envelopes that influence the cortical response.

We found that neurons in AI can be tuned to specific features of the sinusoidal spectral envelope of a complex sound, including the spacing of the spectral maxima and minima and the depth of spectral modulation or intensity contrast. In addition, the position of the spectral envelope relative to the standard receptive field is relevant, that is, the intensity and the phase of the spectral envelope affect the response. Carrier signal parameters of the spectral envelope signal, such as bandwidth and spectral density, play a role in shaping the cortical response as well.

Single Unit Versus Multiple Unit Recordings

Before discussing the results of this study in the context of auditory coding strategies, a brief consideration will be given to some methodological issues. Since these are among the first parametric experiments to explore the responses of cortical cells to characteristics of the spectral envelope, we chose to record from both single and multiple neurons. The main reason was the relatively large number of stimulus parameters that needed to be

FIGURE 9 **Intensity shifts.** Responses of units as a function of the overall intensity. The stimuli all had a modulation depth of 30 dB, and the following recording site characteristics and ripple densities (rd) (A) single unit, rd = 1.0; (B) single unit, rd = 1.0; (C) single unit, rd = 1.0; (D) single unit, rd = 0.9; (E) multiple unit, rd = 0.9; (F) single unit, rd = 1.0.

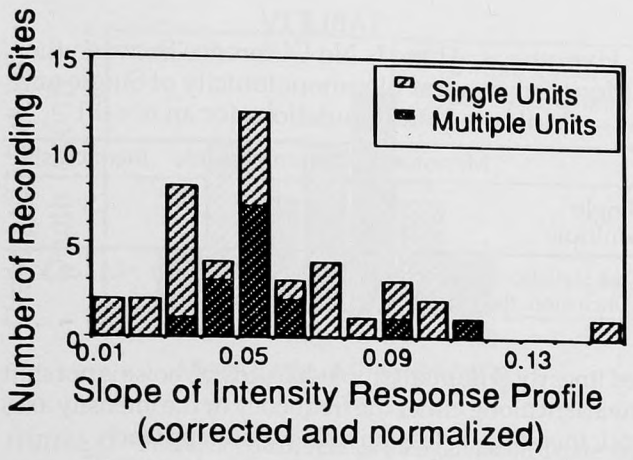

FIGURE 10 **Frequency distribution of dynamic range of units.** The positive slope of the intensity response profile indicates the dynamic range of the neurons. To normalize the response, the slope was divided by the difference between the maximum and minimum number of spikes. The light hatching represents 28 single units and the dark hatching represents 15 multiple units. The bin size is 0.01.

systematically tested for each recording site. Since the isolation of single units is more difficult to maintain over an extended period of time, the use of multiple unit recordings yielded a higher percentage of locations that were completely characterized for single-tone, two-tone, and ripple stimuli. The mean and variance of the best ripple density of recording sites, the shape and bandwidth of the RTF, and the monotonicity of the intensity response profile were found to be similar for single and multiple unit recordings. Consequently, multiple and single unit results are discussed conjointly. However, the distinct differences between the two recording methods and their potential influence on the interpretation should be kept in mind (for discussion see Schreiner and Mendelson, 1990). Since some characteristics of pure-tone frequency response areas, such as sharpness of tuning (Schreiner and Sutter, 1992) and monotonicity of rate-level functions (Sutter and Schreiner, in press) can show distinct differences between the results from these two recording methods, the similarity of the results obtained from single and multiple units for these broadband stimuli is noteworthy. The similarity between the group response and the element response may be an indication that more complex stimuli, such as ripple stimuli, are better suited than pure tones for the study of local cortical properties, since they may engage and reveal more fully the cooperation within the local neuronal population. Since the responses were obtained from the middle laminae, no clear test of a potential columnar organization was possible. However, an indication of nonuniform spatial distributions along the isofrequency domain was evident, suggesting that the spatial frequency analysis is locally and globally not randomly distributed.

Acoustic Stimulus: Carrier and Spectral Envelope

As pointed out in the "Introduction", arguments for the use of ripple spectra in the exploration of cortical processing come from the study of the visual cortex, from recent psychoacoustical studies that focused on the coding of spectral envelopes, and from system-theoretical considerations.

Both temporally and spatially complex stimuli have been used for the highly advanced investigation of signal coding in the visual cortex (see Maffei and Fiorentini, 1973; Albrecht and DeValois, 1981). It has been shown in the visual system that certain tuning properties of a neuron vary with some other stimulus properties. The sharpness of directional orientation tuning, for example, is dependent on whether the stimulus is a long bar or a wide bar. It has also been suggested that dividing neurons into categories based on response properties is dependent on the stimulus used (Maffei and Fiorentini, 1976; Hammond and Munden, 1990). Of particular interest in this context are studies that utilize luminance gratings to explore the properties of visual cortical neurons (Maffei and Fiorentini, 1976; Zhang, 1990; Jagadeesh *et al.*, 1993, for review see DeValois and De Valois, 1990). By using the response to sinusoidal luminance gratings as a basis for a general characterization, the response of many simple cells to various visual stimuli has proven to be predictable (Campbell and Robson, 1968; Worgotter and Eysel, 1987; De Angelis *et al.*, 1993; Jagadeesh *et al.*, 1993). In this case, stimuli excite a wide range of the receptor surface (the retina) in contrast to spatially restricted light points or bars. By manipulating the characteristics of the gratings, a number of receptive field properties can be evaluated that take into account long range and short range spatial influences and interactions. This approach is based on the system-theoretical equivalence of a system impulse response and system transfer or filter function applied to the spatial domain of the receptor surface. By presenting different spatial frequency gratings and taking the Fourier transform of the resulting transfer function, estimations of the impulse response (the receptive fields) for simple cells can be obtained. Although investigations on the visual cortex have had great success determining and explaining receptive field properties by rigorously applying parametrically accessible stimuli under system-theoretical considerations, little of that approach has been transferred to the exploration of the central auditory system.

Early physiological studies investigating effects of the spectral envelope on auditory responses used a ripple-like stimuli, "cosine noise" (de Boer, 1967; Evans *et al.* 1970; Bilsen and Goldstein, 1974; Bilsen *et al.*, 1975). By delaying white noise and adding it to itself, a broadband stimulus was created with a sinusoidal spectral envelope and a carrier of noise. The resulting stimulus had linearly spaced peaks and a spectral envelope amplitude that var-

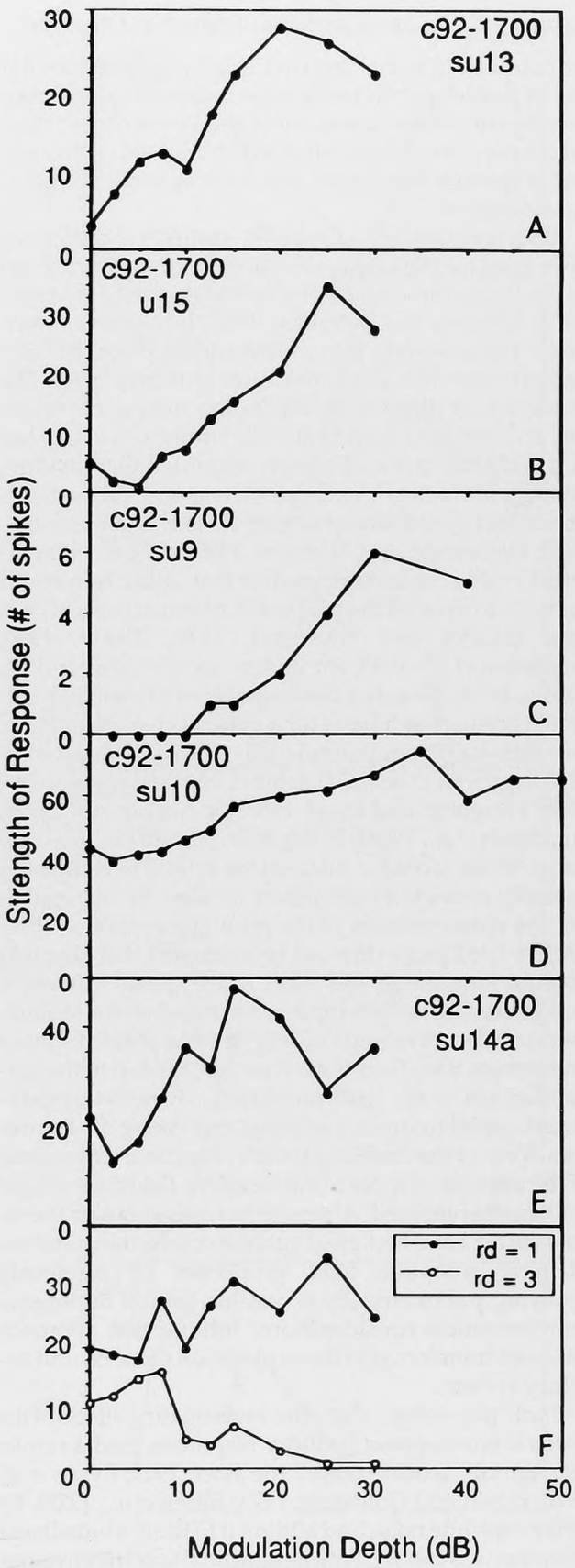

TABLE IV
Hypothesis: There Is No Difference Between the Monotonicity and Nonmonotonicity of Single and Multiple Unit Populations for an $\alpha = 0.1$

	Monotonic	Nonmonotonic	Inconclusive
Single	3	18	7
Multiple	5	7	2

Test statistic = 3.88; critical value = 7.77 (for $\alpha > 0.1$, df = 4). Conclusion: the hypothesis is not rejected.

ied linearly. Although ripple-like, cosine noise is not shift invariant along either the frequency or the intensity axes and, therefore, is less suitable for our approach.

Later, psychophysical studies used spectrally complex stimuli to address the perception of spectral profiles (Bernstein and Green, 1988; Berg and Green, 1990; Green and Berg, 1991) and the influence of spectrally more distant regions on the processing and perception of presumably locally derived attributes (Hall *et al.*, 1984; Moore and Shailer, 1991; Richards and Heller, 1991). The sinusoidal spectral envelope has been used in a few psychoacoustical studies either to study the effects of spectral peak spacings (Houtgast, 1977; Hillier, 1991; Schreiner *et al.*, 1993; Shamma *et al.*, 1994), and to study spectral motion after-effects (Shu *et al.*, 1993). Testing the effectiveness of a ripple stimulus as a forward or direct masker, Houtgast (1977) showed psychoacoustically that not only the spacing of the peaks, but also the phase of the spectral envelope is important. Investigating whether there are segregated "channels" in the auditory system for taking the Fourier transform of the spectral envelope, Hillier (1991) found evidence for independent encoding of different ripple densities. Although these studies reveal several similarities between the behavior of the auditory system and that of the visual system, when using comparable stimulus features, no directly corresponding physiological studies have been undertaken that could account for the psychophysical observations.

The success in the visual system of elucidating receptive field properties and perceptual phenomena with spatially complex stimuli that satisfy certain system-theoretical constraints, and the importance of spectral envelopes in discriminating vocalizations, particularly vowels, suggests a similar investigation of the spatial dimension of sounds, relative to the receptor surface, and their relationship to frequency organization. The results of such an approach provide an expansion of the possi-

FIGURE 11 **Modulation depth response profiles.** Responses of six typical units as the modulation depth of the stimulus is varied. Details of the stimulus and recording site were (A) single unit, ripple density (rd) = 1.0; (B) multiple unit, rd = 1.0; (C) single unit, rd = 1.0; (D) single unit, rd = 0.33; (E) single unit, rd = 1.5; (F) multiple unit. (Closed circles, rd = 1.0; open circles, rd = 3.0 ripples/octave.)

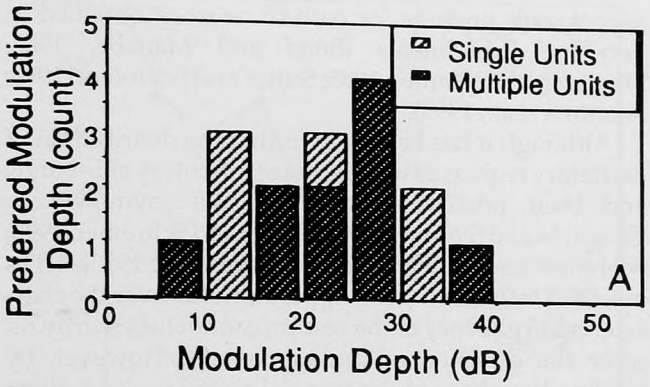

FIGURE 12 **Frequency distributions for modulation depth.** The histogram shows the frequency distribution for preferences in the modulation depth. The lightly shaded bars represent single units (n = 6), and the darkly shaded bars represent multiple units (n = 10).

bilities to characterize neuronal response properties, should allow an assessment whether pure-tone receptive fields are sufficient to predict the response to spectrally complex signals, and may reveal new insights into the principles underlying the representation of complex sounds in the auditory cortex.

Ripple Transfer Functions

Previous studies have used tonal stimuli to evaluate the receptive fields of neurons. Pure-tone receptive fields allow the characterization of the response selectivity of neurons by extracting descriptive parameters, such as characteristic frequency, minimum threshold, and the bandwidth of the tonal response. Although such a characterization can be sufficient to predict the response of a peripheral neuron to a variety of stimuli, there is ample evidence that central neurons have stimulus selectivities that are not predictable from pure-tone responses alone. Examples include selective responses to complex sonar signals in bat auditory cortical neurons (Suga, 1965), vocalization-specific neurons in squirrel monkeys (Newman and Wollberg, 1973a,b), song-selective neurons in birds (Langner *et al.*, 1981), and syllable sensitivity in human cortical neurons (Creutzfeldt *et al.*, 1989). To systematically explore potential response selectivities of cortical neurons beyond frequency and intensity, other stimulus dimensions that may be of relevance to the animal must be utilized. Transfer functions, intensity response profiles, and phase response profiles of ripple spectra provide a systematic characterization of neuronal responses that may reveal additional aspects of receptive fields while reflecting some of the properties seen with pure-tone responses. Although a thorough correlational analysis between RTF properties and pure-tone frequency response areas will be presented elsewhere, a brief discussion on the concepts and interpretations of RTF properties with regard to traditional tuning curves will be outlined. For the following discussion of observed RTF properties, it will suffice to consider only a few of the most common aspects of frequency response areas, namely, the width and strength of a central excitatory area and the position and strength of flanking inhibitory sidebands.

In this portion of the study, RTFs were exclusively obtained for the cosine phase of the spectral envelope, that is, a spectral maximum was located at the CF of the neurons. For this condition, four characteristics of RTFs were used to describe the variance in the obtained sample: the overall shape of the RTF, the ripple density producing the strongest response, the bandwidth of the RTF, and the degree of response modulation due to changes in the spectral envelope frequency.

The occurrence of the two most common types of RTF shape, band pass and low pass, representing 67% of the sample, can be largely attributed to the presence of relatively strong inhibitory sidebands in the FRAs. With the center peak of the ripple stimulus aligned with the CF of the unit, the maximum response to the stimulus will be attained when the neighboring spectral minima are positioned to coincide with the inhibitory sidebands. If the ripple density is lowered or increased, the invoked inhibition will increase by expanding the central peak into the sidebands or by moving neighboring ripple maxima into the inhibitory sidebands, respectively, thus creating a band-pass characteristic of the RTF. RTFs with low-pass characteristics can be seen when inhibitory sidebands are absent or only weak. Other RTF filter shapes are probably also related to the spacing and relative strength of excitatory and inhibitory regions. Asymmetries in the arrangement and strength of these portions of the FRAs are likely contributing to the creation of notch or irregularly shaped RTFs. It has been shown (Suga and Manabe, 1982; Sutter and Schreiner 1990; Shamma *et al.*, 1993) that the strength and relative position of the excitatory and inhibitory regions can vary substantially between neurons. Thus, the different receptive field organizations required to create the observed RTFs of varied shapes do exist.

Another important descriptor of RTFs relates to the position of the peak or the upper cutoff along the ripple density axis. These aspects of RTFs reflect both the width of the classic excitatory receptive field and the distance of the inhibitory sidebands from the center of the excitatory portion. Neurons showing a preference for higher ripple densities are likely to have narrow tuning curves and more closely spaced inhibitory sidebands. By contrast, preferences for low ripple densities probably reflect more broadly tuned neurons that, as a consequence, have fairly widely spaced inhibitory sidebands. The best ripple densities between 0.5 and 4 ripples per octave, as seen for the majority of neurons in this study, indicate that spacings between inhibitory and excitatory regions in neurons can vary between 0.25 and 2 octaves, con-

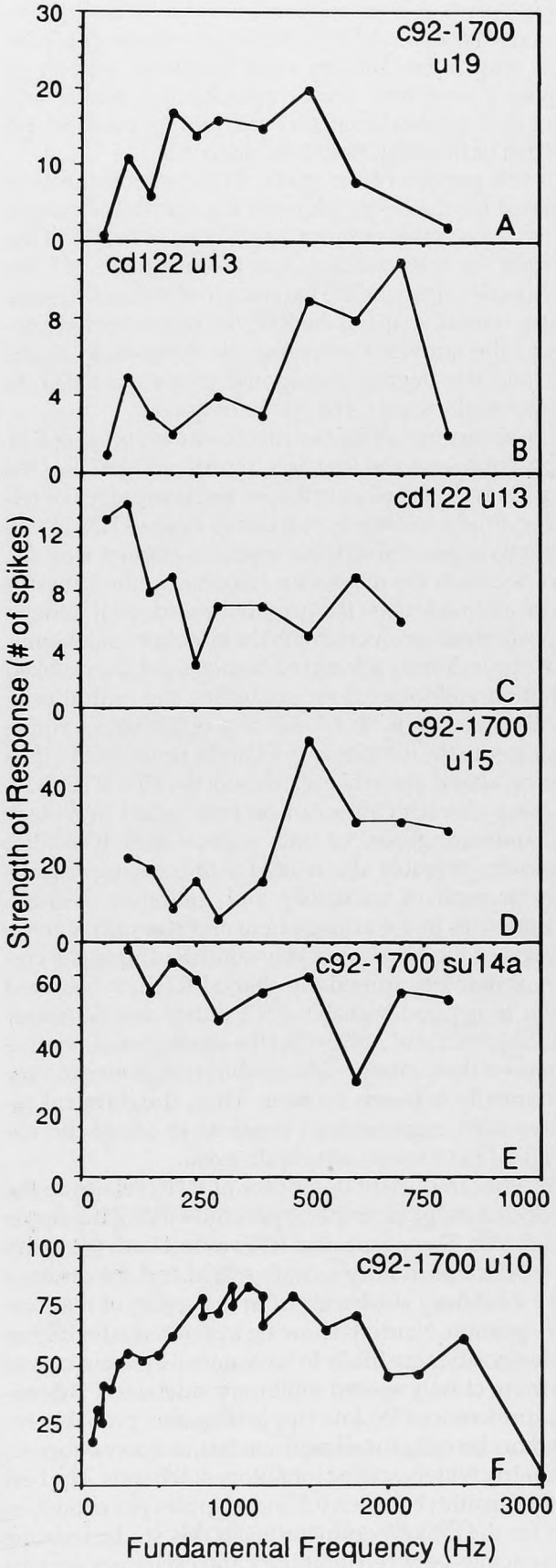

sistent with findings for cortical neurons obtained in two-tone experiments (Suga and Manabe, 1982; Shamma and Symmes, 1985; Sutter and Schreiner, 1990; Shamma *et al.*, 1993).

Although it has been shown that the distribution of excitatory regions as well as that of inhibitory side bands and their relative strength can be asymmetrical, (Shamma and Symmes, 1985; Sutter and Schreiner, 1990; Schreiner and Sutter, 1992; Shamma *et al.*, 1993), RTFs obtained by centering the ripple stimulus over the characteristic frequency of the neuron cannot necessarily resolve the direction of the asymmetry. However, by varying the phase of the spectral envelope for a given ripple density or by obtaining RTFs for different phases, some of these asymmetries can be investigated (see later).

The interpretive value of two other descriptors of RTFs, the bandwidth and the modulation index RMI, is more difficult to assess. The modulation index is an indicator of the neuron's variation in activity due to changes in the ripple density of the spectral envelope. A high modulation index suggests a relatively high efficacy of excitatory or inhibitory influences of surrounding areas on the response strength of a neuron or a large change in the response strength with small (about 6 dB) changes in intensity. A low modulation index suggests relatively weak excitatory and inhibitory influences from surrounding areas, or not much change in the strength of the response with small changes in intensity. The bandwidth of RTFs also reflects these properties but, in addition, incorporates aspects related to the spacing of excitatory and inhibitory regions that are more directly expressed by the best ripple density or the upper cutoff density.

A useful feature to distinguish vowels independent of speaker gender or age is to consider the frequency ratio of the formants (Miller, 1989). Depending on the vowel, most formants are spaced between 0.3 and 4.0 octaves, with the majority of ratios clustering around 1 octave. The best ripple densities of the neurons in AI in this study covered a similar range, with the majority tuned around 1 ripple/octave. Preliminary analysis of cat vocalizations (see Fig. 1) also indicates, similar to human vowels, a preponderance of formant ratios around 1 octave.

FIGURE 13 **Fundamental frequency response profiles.** Change of response magnitude at best ripple density as a function of fundamental frequency. The characteristic frequencies (cf) for these neurons ranged from 4.6 to 7.5 kHz. Details of the recording site and the stimuli: (A) multiple unit, cf = 4.6 kHz; rd = 1.0; (B) multiple unit, cf = 5.5 kHz, rd = 3.0; (C) multiple unit, cf = 5.5 kHz, rd = 1.0; (D) multiple unit, cf = 6.9 kHz, rd = 1.0; (E) single unit, cf = 6.5 kHz, rd = 1.5; (F) single unit, cf = 7.5 kHz, rd = 0.33 ripples/octave.

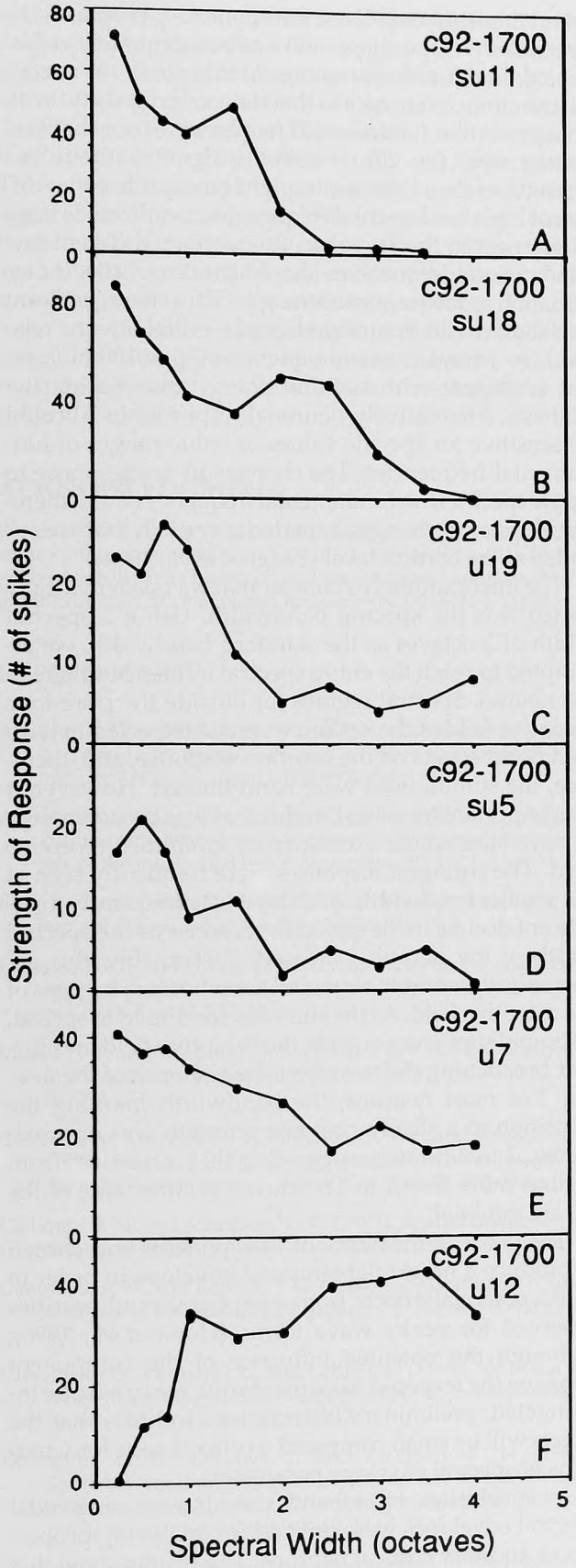

Taken together, the characteristics of cosine RTFs reflect a number of receptive field properties that have been observed with pure-tone or two-tone measurements of FRAs. In addition, the RTF may provide information that is usually not reflected in FRAs, namely, the cumulative effect of excitatory and inhibitory influences on the response strength, including effects from regions outside the classic receptive field.

Response Profiles

The various parameters of the ripple stimulus that were controlled included the phase of the spectral envelope, the modulation depth, the spacing of the components, the bandwidth of the stimulus, and the overall intensity.

Variations of the phase of the spectral envelope invariably had a large effect on the magnitude of the response. It is known from pure-tone stimuli that the characteristic frequency is bordered by regions that are either inhibitory or nonresponsive. Thus, it would be expected that the strongest response to a ripple stimulus would be for a stimulus with a maximal amount of energy near the CF, and a minimal amount of energy in the bordering regions, especially those corresponding to inhibitory areas. Since one of the goals of this particular stimulus was to cover the entire spectral range which might influence the response of a cell, the center peak of the stimulus was positioned at the CF of the unit, covering frequencies 1.5 octaves on either side. Changes in the ripple phase for a fixed ripple density should reveal whether this position was indeed producing the strongest response. Only very few phase profiles showed secondary peaks or a peak significantly shifted from the 0° position. That is, the alignment of a spectral maximum with the CF was near optimal. Slight deviations in the phase profile of the maximum from zero may be accounted for by discrepancies between the BF of a neuron at the stimulus intensity that corresponded to the local energy of the ripple stimulus and the near threshold estimate of the CF.

If the filtering system reflected in the RTFs were linear and symmetrical, the phase response profile for a given ripple density would be sinusoidal (the profiles would match the sinusoidal patterns, hatched lines in Fig. 7). The clear deviations from the sinusoidal profile in all the phase profiles is a strong indication of either nonlinear components or asymmetries in the filter. Differences in the symmetry of the phase profiles are likely closely related to the asymmetries in the distribution and strength of inhibitory sidebands as shown

FIGURE 14 **Spectral width response profiles.** Six typical spectral width response profiles are shown. (A) Single unit, rd = 1.66; (B) single unit, rd = 1.0; (C) multiple unit, rd = 1.0; (D) single unit, rd = 1.0; (E) multiple unit, rd = 1.0; (F) single unit, rd = 5.0 ripples/octave.

with two-tone stimuli for AI neurons (Sutter and Schreiner 1990, 1991; Shamma *et al.*, 1993). Equal numbers of positive and negative asymmetries suggest an equal number of neurons with stronger high- and low-frequency inhibitory sidebands (Shamma *et al.*, 1993).

As the spectral modulation depth of a stimulus with fixed and near optimal ripple density was systematically increased, the responses usually increased up to a constant value. However, on some occasions responses decreased with increasing modulation depth. The most likely explanation for this difference in response behavior with changes in modulation depth is again related to the presence and strength of influence by inhibitory sidebands. If strong sidebands are present, an increase in the modulation depth of the optimally positioned spectral envelope will mostly decrease the input to the inhibitory sidebands while maintaining the input to the central excitatory region. However, if no or only weak inhibition is present or if the spectral envelope is not optimally positioned, an increase in the modulation depth may remove excitatory energy from the receptive field and, thus, reduce the response strength. Most neurons showed the greatest changes in responsiveness for modulation depths between 5 and 25 dB. For a reference on spectral modulation depth sizes, vowels usually have spectral modulation depths of 10 to 30 dB between formants, the same range where the neurons were most sensitive to change in the modulation depth of the spectral envelope.

As a function of overall intensity, the neurons predominantly behaved in a nonmonotonic manner in response to ripple stimuli. This behavior contrasts with that seen in response to pure-tone stimuli. Using pure tones, various portions of sampled neurons in AI (24 to 60%) have been reported to have shown nonmonotonic behavior (Phillips *et al.*, 1985, 1989; Schreiner *et al.*, 1992). The finding here that 76% of the neurons showed nonmonotonic rate or level functions for ripple stimuli suggests that neurons are more selective or more sharply tuned to specific signal intensities when stimulated with broadband stimuli than with narrowband stimuli. Similarly, a high percentage of nonmonotonic rate or level functions have been found by Imig and colleagues (1990) for free-field wideband noise stimuli. Both observations are consistent with the hypothesis that the activation of inhibitory sidebands plays a major role in creating intensity selectivity (Phillips, 1988).

As was seen, there are considerable changes in the response as the fundamental frequency of the carrier band varies over a limited range. As the fundamental frequency is varied, the number of components per octave or per critical band varies. However, as long as the fundamental frequency is small, the energy per octave or per critical band remains fairly constant. As the fundamental frequency increases, there are fewer components per octave or per critical band. In the extreme case, when there are only a few components per octave, the spectral envelope shape will not be adequately represented due to undersampling. At this point, the energy distribution over critical bands varies greatly with changes in the fundamental frequency. Since the local energy near the CF contributes significantly to the strength of the response, it might be expected that different high fundamental frequencies can produce large differences in the response. By contrast, different low fundamental frequencies should produce little, if any, variation in the response strength. Thus, the significant variations in the response strength, even between relatively low fundamental frequencies (50 to 100 Hz), are not consistent with such an energy distribution hypothesis. Alternatively, neuronal responses in AI could be sensitive for specific values or value ranges of fundamental frequencies. The changes in the response to ripple spectra with fundamental frequency could, therefore, be due to changes in periodicity pitch that are encoded at the cortical level (Langner *et al.*, 1994).

The final stimulus parameter that was systematically varied was the spectral bandwidth. Using a spectral width of 3 octaves as the standard bandwidth, we attempted to reach the entire spectral influence sphere of the neuron. Spectral regions far outside the pure-tone receptive field of the neuron were not expected to have significant effects on the neuron's response, and, therefore, the stimuli used were band-limited. However, it was important to use a stimulus that was broad enough to cover the whole excitatory or inhibitory receptive field. The strongest responses were frequently seen at the smaller bandwidths and there was frequently a significant decline in the neuron's response as the spectral width of the neuron increased. Presumably, this occurred as the stimulus invaded the inhibitory regions of the receptive field. As the stimulus continued to spread, its boundaries were outside the receptive field and further broadening did not affect the response of the neuron. For most neurons, the bandwidth marking the transition to a steady response strength was approximately 2 to 3 octaves, suggesting that influences from regions more than 1 to 1.5 octaves to either side of the CF are minimal.

The phase of the harmonic components was chosen to produce a nearly flat temporal envelope in order to avoid potential effects from peripheral nonlinearities observed for peaky wave forms (Horst *et al.*, 1990). Although the potential influence of the component phase on the response to ripple stimuli remains to be investigated, preliminary observations indicate that the effects will be small compared to effects seen for variations of spectral envelope parameters.

In conclusion, broadband stimuli with sinusoidal spectral envelopes were utilized for analyzing properties of auditory cortical neurons. The results show that the neuron's responses are sensitive, if not selective, to

specific aspects of the spectral envelope, such as the spatial frequency, ripple phase, or ripple depth. The results suggest that cortical neurons can represent the shape of broadband stimuli in the form of a spatial Fourier analysis of the spectral envelope. The conclusions drawn from the RTFs are limited by the use of only one ripple phase. To characterize completely a neuron's response, each spectral envelope frequency must be presented at least for two orthogonal phases (such as 0 and 90°) so that it analyzes the symmetrical properties of the neurons' response as well as the asymmetrical properties. In addition, any possible relationships between traditional pure-tone tuning curves, and these response profiles must be investigated. We will be addressing these aspects in the future.

ACKNOWLEDGMENT

We thank Drs. D. Keeling and K. Krueger, who participated in some of the experiments, and Dr. G. Langner for reviewing an earlier version of the manuscript. This study was supported by a grant from the Office of Naval Research (N00014-91-J-1317).

REFERENCES

Albrecht, D. G. and DeValois, R. L. (1981). Striate cortex responses to periodic patterns with and without fundamental harmonics. *J. Physiol. (Lond.) 319*, 497–514.

Asanuma, A., Wong, D. and Suga, N. (1983). Frequency and amplitude representations in the anterior primary auditory cortex of the mustached bat. *J. Neurophys. 50*, 1182–1196.

Berg, B. G. and Green, D. M. (1990). Spectral weights in profile listening. *J. Acoust. Soc. Am. 88*, (2)758–66).

Bernstein, L. R. and Green, D. M. (1988). Detection of changes in spectral shape: uniform vs. non-uniform background spectra. *Hear. Res. 32*, 157–66.

Bilsen, F. A. and Goldstein, J. L. (1974). Pitch of dichotically delayed noise and its possible spectral basis. *J. Acoust. Soc. Am. 55*, 292–296.

Bilsen, F. A., Ten Kate, J. H., Buunen, T. J. F. and Raatgever, J. (1975). Responses of single units in the cochlear nucleus of the cat to cosine noise. *J. Acoust. Soc. Am. 58*, 858–866.

Calhoun, B. M. and Schreiner, C. E. (1993). Spatial frequency filters in cat auditory cortex. *Soc. Neurosci. Abstr., 23*, 581.8.

Campbell, F. W. and Robson, J. G. (1968). Application of Fourier analysis to the visibility of gratings. *J. Physiol. (Lond.) 197*, 551–166.

Creutzfeldt O., Ojemann, G. and Lettich, E. (1989). Neuronal activity in the human lateral temporal lobe. I. Responses to speech. *Exp. Brain Res. 77*, 451–475.

DeAngelis, G. C., Ohzawa, I. and Freeman, R. D. (1993). Spatiotemporal organization of simple-cell receptive fields in the cat's striate cortex. II. Linearity of temporal and spatial summation. *J. Neurophys. 69*, 1118–1135.

de Boer, E. (1967). Correlation studies applied to the frequency resolution of the cochlea. *J. Aud. Res. 7*, 209–217.

De Valois, R. L. and De Valois, K. K. (1990). *Spatial Vision*. Oxford University Press, New York.

Dickson, D. P. and Maue-Dickson, W. (1982). *Anatomical and Physiological Bases of Speech*. Little, Brown & Company, Boston.

Eggermont, J. J. (1993). Differential effects of age on click-rate and amplitude modulation-frequency coding in primary auditory cortex of the cat. *Hear. Res. 65*, 175–192.

Evans, E. F., Rosenberg, J. and Wilson, J. P. (1970). The effective bandwidth of cochlear nerve fibres. *J. Physiol. (Lond.) 207*, 62P–63P.

Green, D. M. and Berg, B. G. (1991). Spectral weights and the profile bowl. *Quar. J. Exp. Psychol. 43*, 449–458.

Hall, J. W., Haggard, M. P. and Fernandes, M. A. (1984). Detection in noise by spectro-temporal pattern analysis. *J. Acoust. Soc. Am. 76*, 50–56.

Hammond, P. and Munden, I. M. E. (1990). Areal influences on complex cells in cat striate cortex: Stimulus-specificity of width and length summation. *Exp. Brain Res. 80*, 135–147.

Heil P., Langner, G. and Scheich, H. (1992a). Processing of frequency-modulated stimuli in the chick auditory cortex analogue: Evidence for topographic representations and possible mechanisms of rate and directional sensitivity. *J. Comp. Physiol. 171A*, 583–600.

Heil, P., Rajan, R. and Irvine, D. R. F. (1992b). Sensitivity of neurons in cat primary auditory cortex to frequency-modulated stimuli. II: Organization of response properties along the 'isofrequency' dimension. *Hear. Res. 63*, 135–150.

Hillier, D. A. (1991). *Auditory Processing of Sinusoidal Spectral Envelopes*. Doctoral Thesis. Washington University, St. Louis.

Horst, J. W., Javel, E. and Farley, G. R. (1990). Coding of spectral fine structure in the auditory nerve. II. Level-dependent nonlinear responses. *J. Acoust. Soc. Am. 88*, 2656–2681.

Hose B., Langner, G. and Scheich, H. (1987). Topographic representation of periodicities in the forebrain of the mynah bird: One map for pitch and rhythm? *Brain Res. 422*, 367–373.

Houtgast, T. (1977). Auditory-filter characteristics derived from direct-masking data and pulsation-threshold data with a rippled-noise masker. *J. Acoust. Soc. Am. 62*, 409–415.

Imig, T. J. and Adrian, H. O. (1977). Binaural columns in the primary field (A1) of cat auditory cortex. *Brain Res. 138*, 241–257.

Imig, T. J., Irons, W. A. and Samson, F. R. (1990). Single-unit selectivity to azimuthal direction and sound pressure level of noise bursts in cat high-frequency primary auditory cortex. *J. Neurophysiol. 63*, 1448–1466.

Jagadeesh, B., Wheat, H. S. and Ferster, D. (1993). Linearity of summation of synaptic potentials underlying direction selectivity in simple cells of the cat visual cortex. *Science, 262*, 1901–1904.

Langner, G., Bonke, D. and Scheich, H. (1981). Neuronal discrimination of natural and synthetic vowels in field L of trained mynah birds. *Exp. Brain Res. 43*, 11–24.

Langner, G., Sams, M., Heil, P., McEvoy, L. K., Hari, R. and Ahonen, A. (1994). Periodicity pitch is represented topographically in the human auditory cortex: Evidence by magnetoencephalography. *Gottingen Neurobiol. Rep. 2*, 388.

Maffei, L. and Fiorentini, A. (1973). The visual cortex as a spatial frequency analyser. *Vision Res. 13*, 1255–1267.

Maffei, L. and Fiorentini, A. (1976). The unresponsive regions of visual cortical receptive fields. *Vision Res. 16*, 1131–1139.

Mendelson, J. R. and Cynader, M. S. (1985). Sensitivity of cat primary auditory cortex (A1) neurons to the direction and rate of frequency modulation. *Brain Res. 327*, 331–335.

Mendelson, J. R. and Grasse, K. L. (1992). A comparison of monaural and binaural responses to frequency modulated (FM) sweeps in cat primary auditory cortex. *Exp. Brain Res. 91*, 435–454.

Mendelson, J. R., Schreiner, C. E., Sutter, M. S. and Grasse, K. L. (1993). Functional topography of cat primary auditory cortex: responses to frequency-modulated sweeps. *Exp. Brain Res. 94*, 65–87.

Merzenich, M. M., Knight, P. L. and Roth, G. L. (1975). Representation of cochlea within primary auditory cortex in the cat. *J. Neurophys. 38*, 231–249.

Middlebrooks, J. C., Dykes, R. W. and Merzenich, M. M. (1980). Binaural response-specific bands in primary auditory cortex (A1) of the cat: Topographical organization orthogonal to isofrequency contours. *Brain Res. 181*, 31–48.

Miller, J. D. (1989). Auditory-perceptual interpretation of the vowel. *J. Acoust. Soc. Am. 85*, 2114–2134.

Moore, B. C. J. and Shailer, M. J. (1991). Comodulation masking release as a function of level. *J. Acoust. Soc. Am. 90*, 829–835.

Newman, J. D. and Wollberg, Z. (1973a). Multiple coding of species-specific vocalizations in the auditory cortex of squirrel monkeys. *Brain Res. 54*, 287–304.

Newman, J. D. and Wollberg, Z. (1973b). Responses of single neurons in the auditory cortex of squirrel monkeys to variants of a single call type. *Exp. Neurol. 40*, 821–824.

Phillips, D. P. (1988). Effect of tone-pulse rise time on rate-level functions of cat auditory cortex neurons: Excitatory and inhibitory processes shaping responses to tone onset. *J. Neurophysiol. 59*, 1524–1539.

Phillips, D. P. and Hall, S. E. (1987). Responses of single neurons in cat auditory cortex to time-varying stimuli: Linear amplitude modulations. *Exp. Brain Res. 67*, 479–492.

Phillips, D. P., Hall, S. E. and Hollett, J. L. (1989). Repetition rate and signal level effects on neuronal responses to brief tone pulses in cat auditory cortex. *J. Acoust. Soc. Am. 85*, 2537–2549.

Phillips, D. P. and Irvine, D. R. F. (1981). Responses of single neurons in physiologically defined primary auditory cortex (A1) of the cat: Frequency tuning and responses to intensity. *J. Neurophysiol. 45*, 48–58.

Phillips, D. P., Orman, S. S., Musicant, A. D. and Wilson, G. F. (1985). Neurons in the cat's primary auditory cortex distinguished by their responses to tones and wide-spectrum noise. *Hear. Res. 18*, 73–86.

Raggio, M. and Schreiner, C. E. (1994). Neuronal responses in cat primary auditory cortex to electrical cochlear stimulation: I. Intensity dependence of firing rate and response latency. *J. Neurophysiol. 72*, 2334–2359.

Rajan, R., Aitkin, L. M., Irvine, D. R. and McKay, J. (1990a). Azimuthal sensitivity of neurons in primary auditory cortex of cats. I. Types of sensitivity and effects of variations in stimulus parametres *J. Neurophysiol. 64*, 872–887.

Rajan, R., Aitkin, L. M. and Irvine, D. R. (1990b). Azimuthal sensitivity of neurons in primary auditory cortex of cats. II. Organization along frequency-band strips. *J. Neurophysiol. 64*, 888–902.

Reale, R. A. and Imig, T. J. (1980). Tonotopic organization in auditory cortex of the cat. *J. Comp Neurol. 192*, 265–291.

Richards, V. M. and Heller, L. M. (1991). The detection of a tone added to a narrow band of noise: The energy model revisited. *Q. J. Exp. Psychol. 43*, 481–501.

Schreiner, C. E., Calhoun, B. and Keeling, D. (1993). Physiology and topography of cortical neurons explored with vowel-like ripple-spectra. *Assoc. Res. Otolaryngol. Abstr. 16*, 161.

Schreiner, C. E., Mendelson, J. R. and Sutter, M. L. (1992). Functional topography of cat primary auditory cortex: distribution of tone intensity. *Exp. Brain Res. 92*, 105–122.

Schreiner, C. E. and Mendelson, J. R. (1990). Functional topography of cat primary auditory cortex: distribution of integrated excitation. *J. Neurophysiol. 64*, 1442–1459.

Schreiner, C. E. and Sutter, M. L. (1992). Topography of excitatory bandwidth in cat primary auditory cortex: single-neuron versus multiple-neuron recordings. *J. Neurophysiol. 68*, 1487–1502.

Schreiner, C. E. and Urbas, J. V. (1988). Representation of amplitude modulation in the auditory cortex of the cat. II: Comparison between cortical fields. *Hear. Res. 32*, 49–64.

Shamma, S. A., Fleshman, J. W., Wiser, P. R. and Versnel, H. (1993). Organization of response areas in ferret primary auditory cortex. *J. Neurophysiol. 89*, 367–383.

Shamma, S. A. and Symmes, D. (1985). Patterns of inhibition in auditory cortical cells in awake squirrel monkeys. *Hear. Res. 19*, 1–13.

Shamma, S. A., Versnel, H. and Kowalski, N. (1994). Responses to rippled complex sound stimuli in primary auditory cortex. *Assoc. Res. Otolaryngol. Abstr. 17*, 86.

Shu, Z. G., Swindale, N. V. and Cynader, M. S. (1993). Spectral motion produces an auditory after-effect. *Nature 364*, 721–723.

Suga, N. (1977). Amplitude spectrum representation in the Doppler-shifted-CF processing area of the auditory cortex of the mustache bat. *Science 196*, 64–76.

Suga, N. (1965). Functional properties of auditory neurones in the cortex of echo-locating bats. *J. Physiol. (Lond.) 181*, 671–700.

Suga, N. and Jen, P. H. S. (1976). Disproportionate tonotopic representation for processing CF-FM sonar signals in the mustache bat auditory cortex. *Science 194*, 542–544.

Suga, N. and Manabe, T. (1982). Neural basis of amplitude-spectrum representation in auditory cortex of the mustached bat. *J. Neurophysiol. 47*, 225–255.

Sutter, M. L. and Schreiner, C. E. (1990). Two-tone responses of single units in cat primary auditory cortex. *ARO Abstr. 13*, 221.

Sutter, M. L. and Schreiner, C. E. (1991) Physiology and topography of neurons with multipeaked tuning curves in cat primary auditory cortex. *J. Neurophysiol. 65*, 1207–1226.

Sutter, M. L. and Schreiner, C. E. (in press). Topography of intensity parameters in cat primary auditory cortex: single-neuron versus multiple-neuron recordings. *J. Neurophysiol.*

Woolsey, C. N. and Walzl, E. M. (1942). Topical projection of the nerve fibers from local regions of the cochlea in the cerebral cortex of the cat. *Bull. Johns Hopkins Hosp. 71*, 315–344.

Worgotter, F. and Eysel, U. TN. (1987). Quantitative determination of orientational and directional components in the response of visual cortical cells to moving stimuli. *Biol. Cybern. 57*, 349–355.

Zhang, J. (1990). How to unconfound the directional and orientational information in visual neuron's response. *Biol. Cybern. 63*, 135–142.